UNIVERSITY OF GHANA

COLLEGE OF BASIC AND APPLIED SCIENCES

FACULTY OF PHYSICAL AND MATHEMATICAL SCIENCES

PERFORMANCE EVALUATION OF NOISE REMOVAL SCHEMES FOR SKIN LESION DETECTION

BY

MELODY NUNYA KAKRABAH

(ID. NO. 10496432)

THIS THESIS IS SUBMITTED TO THE UNIVERSITY OF GHANA, LEGON IN PARTIAL FULFILMENT OF THE REQUIREMENT FOR THE AWARD OF MASTER OF PHILOSOPHY IN COMPUTER SCIENCE DEGREE

DEPARTMENT OF COMPUTER SCIENCE

JULY 2022

UNIVERSITY OF GHANA

COLLEGE OF BASIC AND APPLIED SCIENCES

FACULTY OF PHYSICAL AND MATHEMATICAL SCIENCES

AN IMPROVED HAIR REMOVAL METHOD FOR DERMOSCOPIC IMAGES TOWARDS IMPROVING SKIN LESION DETECTION AND DIAGNOSIS

BY

MELODY NUNYA KAKRABAH

DEPARTMENT OF COMPUTER SCIENCE

JULY 2022

DECLARATION

Except when specific references to the work of others are made, I, *Melody Nunya Kakrabah*, hereby certify that the contents of this dissertation are original and have not been submitted in whole or in part for consideration for any other degree or qualification in this or any other University. Except as stated in the text and acknowledgements, this dissertation is my own work and contains nothing that is the result of collaboration with others. The Supervisory Committee, as listed below, oversaw supervising this dissertation:

…… 04/June/2022 ……

Melody Nunya Kakrabah — Date

(Candidate)

…… 04/June/2022 ……

Dr. Jamal-Deen Abdulai — Date

(Principal Supervisor)

…… 04/June/2022 ……

Dr. Justice Kwame Appati — Date

(Supervisor)

ACKNOWLEDGEMENTS

Courtesy of my supervisors', my family, and friends' constant encouragement and unwavering support, this work has been able to see the light of day. Thank you all.

ABSTRACT

Clinicians are continually improving their diagnostic abilities in the ever-changing medical field. A proper diagnosis is imperative for further health care delivery decisions. Skin cancers appear as lesions on any part of the skin, although most appearances are on body parts exposed to sunlight. Lesions may be either malignant or benign. The cells in malignant skin lesions can proliferate and spread to other tissues in other body parts. Malignant skin lesions are among the most lethal types of skin cancers, responsible for increased mortality rates. The diagnosis of skin diseases at the preliminary stages has been demonstrated to improve patients' chances of abidance significantly, while the mortality rate for cases with late detection is on the rise. Computer-Aided Diagnostic systems play a very relevant role in thwarting the prevalence of skin cancer-related deaths by assisting in detecting skin lesions and assisting in diagnosis. Image analysis is enhanced by segmented images, highlighting previously undiscovered features of the original image. When detecting skin diseases from dermoscopic images, segmentation is used to separate the region of interest from the background. Lesions hidden behind elements such as hair, blue-white regions, globules, and an unusual pigment network can only be retrieved with accurate lesion border detection. Consequently, the most important phase is lesion segmentation in the early detection of melanoma. Detection of lesion borders in dermoscopy pictures is difficult because of the presence of noise such as skin lines, air bubbles, hairs and reflections. These are capable of causing significant segmentation mistakes when they are not adequately addressed. The existence of hairs is considered one of the most significant stumbling blocks for most algorithms when it comes to proper segmentation. The similarity of the hair color to the surrounding skin region is one of the main reasons for the difficulty. Improperly addressed hairs often tend to be classified as lesions, resulting in inaccurate segmentation and disease classification. In this thesis, selected hair removal and segmentation algorithms are evaluated and the effects of the hair removal method on the output of segmentation are also evaluated. In analyzing and evaluating a leading method for eliminating hairs in dermoscopic images, the dissertation presents an experimental implementation of a sequence of steps curated based on existing studies to improve segmentation results and justify the impact of these hair removal techniques on the output of image segmentation algorithms. This work uses Blackhat morphological filtering and Otsu's method for thresholding and image inpainting to achieve segmentation with notable improvements recorded.

TABLE OF CONTENTS

LIST OF FIGURES

Chapter 1
INTRODUCTION

1.1 Background

Clinicians are continually improving their diagnostic abilities in the ever-changing medical field. It is said that a proper diagnosis is imperative for further health care delivery decisions. In contrast, erroneous ones can unravel wrongful or postponed treatments that can be detrimental to the patient's health and survival. Ameliorating the quality and accessibility of accurate diagnosis is a key objective in the medical field (Qi et al., 2017). Cancer develops when abnormal cells are formed due to old cells growing out of control causing the malfunctioning of the body's normal control mechanism. Different body parts are affected by different types of cancers. The skin is one such body part affected by the overgrowth of cancerous cells in the epidermis. This results from unrepaired damage to the host DNA which triggers mutations (N et al., 2020). These mutations cause an expeditious multiplication of the skin cells which form malignant tumors. There are four (4) main types of skin cancer known as Merkel Cell Carcinoma (MCC), Squamous Cell Carcinoma (SCC), Basal Cell Carcinoma (BCC) and melanoma (Nasir et al., 2018). Skin cancers appear as lesions on any part of the skin, although most appearances are on body parts exposed to sunlight. Lesions may be either malignant or benign. The cells in malignant skin lesions can proliferate and spread to other tissues in other body parts. Malignant skin lesions are among the most lethal types of human skin cancers, responsible for an increased mortality rate (Attia et al., 2017). Benign lesions, however, have a more organized behavior and remain in the affected region only. According to the skin cancer foundation (2022) statistics, one out of every five (5) Americans will develop cancer by 70 years. Despite the daunting statistics, if identified and diagnosed at an early stage, skin cancers can be treated with non-invasive treatment methods that have proven to yield high recovery rates (Lin et al., 2018). The non-invasive imaging technique designed to help diagnose skin cancer is termed dermoscopy. Visualization of the subsurface structures of the skin is carried out with an oil-immersed microscope and incident light. This is done to reveal the details of colors and texture features of the skin for observation and analysis. It has been observed that the diagnostic accuracy of the dermoscopy technique is largely dependent on the expertise and experience of the practitioner (Bi et al., 2016). Despite this challenge, the detection rate through dermoscopy is substantially better than diagnosis with the naked eye. Computer-Aided Diagnostics (CAD) are thus required to eliminate the margin of subjectivity

in skin cancer diagnosis. Basic CAD systems have three (3) main operational steps: image segmentation, feature extraction, and object classification. The feature extraction and classification steps of the CAD process are certainly hinged on the quantitative analysis of the segmented lesion (Ma & Tavares, 2016). It is evident that the segmentation step is essential and largely affects the entire system's output. Based on the state of the skin, the appearance of the skin lesion images differs significantly. Diagnosis of skin diseases at the preliminary stages has been demonstrated to increase the chances of patients' continuance significantly, while the death rate for cases with late detection is on the rise (Burdick et al., 2018). Early diagnosis of skin cancers presents a unique advantage to patients as appropriate treatments begin at the early stages, thus making skin cancers curable when detected early. On the other hand, late diagnosis makes skin diseases more challenging to cure because of their capability to metastasize to other parts of the affected individual's body, leading to death (Alom et al., 2018). According to the American Cancer Society (ACS), skin disease incidences are expected to increase every year. The main challenge for modern dermatology is providing an efficient analysis tool capable of performing high quality noise removal, segmentation, and the classification of skin diseases, which also decreases the amount of time required for diagnosing without trading accuracy. Dermatologists have previously conducted skin lesion image analysis manually, using their experience and discretion as foundations for diagnosis. This process is laborious and resource-intensive, and output is often subjective and error-prone. The need for a more reliable, less subjective, and more accurate technique cannot be overstated. Developing a robust system to cater to all of these will directly improve the time taken to examine and increase diagnosis accuracy (Izadi et al., 2018). Factors such as hair, texture, air bubble, and oil, among others, affect the appearance of lesions in dermoscopic images and these factors are considered noise (Joseph & Panicker, 2017). To efficiently segment the region of the lesion from a dermoscopic image, the noise needs to be removed from the image. The noise removal techniques are often considered pre-processing actions on the image before proper segmentation begins. This thesis focuses on analyzing and evaluating algorithms available to identify and eliminate hair follicles (considered as noise) prior to the segmentation process to improve the feature extraction and classification steps.

1.2 Problem Statement

There are many approaches to improving CAD systems for a more accurate diagnosis of skin cancers. However, the presence of hair in images makes skin cancer borders often undetectable

or indefinite. Visual identification in practice therefore becomes a daunting task for skin cancer experts. Studies further suggest that solving the noise problem computationally with the noise removal schemes thought practical impacts the reliability of the results of the segmentation and classification process (Mishra & Celebi, 2016). When the hair removal algorithms are ineffective, they often lead to poor lesion analysis, disturbing the lesion's patterns and over-segmentation (Zhang et al., 2000), (Salido & Ruiz, 2017). These hair pieces are eliminated to address this challenge in skin cancer recognition and classification tasks. A real-time CAD tool comes with implementing a feature-preserving automatic hair removal method with minimum computational cost. Therefore, to undertake effective lesion analysis of any kind, an efficient and effective hair-removal algorithm is required (Serrano & Acha, 2009). Thus, it is imperative to properly analyze and attempt to improve hair removal schemes in skin lesion segmentation and classification methods.

1.3 Objectives

This thesis' primary focus is to analyze, evaluate and improve on selected hair removal methods for skin lesion images, detection, and segmentation of lesion borders, and consequently to improve the accuracy of classification of skin lesions to inform diagnosis. This work aims at:

- Reducing the noise (hair) in dermoscopic images without compromising information in the image and outputting quality images acceptable for further processing.
- Potentially improving the performance of the selected hair removal algorithms implementations as input for segmentation without restriction on size and shape.
- Improving the accuracy of the outcome of the segmentation of the pre-processed images.

1.4 Outline of Methodology

For the execution of the experiment, the fundamentals of machine learning are revisited in theory. Various hair removal algorithms are studied theoretically by exploring their mathematical foundations. A suitable algorithm is selected at the end of this exploration phase to be improved upon. To improve upon the algorithm chosen, multiple parameters are varied. Each variation is tested to obtain a stable version of the algorithm for testing the theory presented in the introductory section of this thesis. However, to test the theory, a suitable image segmentation algorithm is selected from the set of algorithms evaluated in chapter 2 of this

work. The results of the implementation of the selected segmentation algorithm are recorded. The hair removal algorithm is executed, and the resulting images (pre-processed) are parsed as input to the segmentation algorithm. A comparison between the two sets of results is made to determine the validity of the claims that improving pre-processing algorithms (hair removal methods) has a significantly positive effect on the output of image segmentation algorithms run on skin lesion images.

1.5 Study's Motivations

Many difficult problems in image processing and pattern recognition motivate many active research programs. This thesis is one of such exploratory ventures to find efficient ways of addressing the problem of hair in dermoscopic images before segmentation. More specifically, this thesis is directed at evaluating and improving a selected hair removal scheme in skin cancer imaging. Of all types of cancers globally, skin cancers are one of the most rapidly increasing with a high mortality rate. The success of this research will provide a more efficient hair removal strategy that will facilitate better detection of skin cancers from skin lesion images. Thus, the study seeks to improve the results of image segmentation and disease classification directly. Notably, skin cancers can be averted with a prompt and accurate diagnosis that informs proper and timely treatment. CAD systems thus play a critical role in thwarting the incidence of skin cancer-related deaths. The success of this study will also help decrease the subjectivity in the diagnostic process of skin-related diseases.

1.6 Organization of Chapters

In this section, the format and structure of this thesis are outlined. This work contains six chapters, including conclusions. All chapters in this work follow the same format, introducing the main concepts and a summary of each chapter's contribution to the goal. The chapters collectively illuminate the evolution of ideas from problem definition to solution elaboration and comment on using Computer-Aided Design Systems in detecting and identifying skin lesions. The remaining chapters are as follows; Chapter 2 is a literature review on skin lesion image segmentation. It also presents the most recent methods, tools, and technologies used in image segmentation. Chapter 3 explains the methodology, tools, and techniques prevalent for hair removal. The mathematical foundations of these methods are also enumerated. This

includes hair removal techniques and lesions border segmentation techniques. Chapter 4 describes the implementation of a comprehensive approach which consists of image enhancement through hair removal and the testing of the viability of the hair removal algorithm by proceeding to segmentation for subsequent melanoma identification. The methods enumerated in this chapter are sourced from the various techniques explained in chapter 3. An experimental implementation of select methods is done with improvements to measure the efficiency of the selected methods in removing hair from images and improving segmentation results. The result of the experiment is evaluated in comparison with other state-of-the-art methods. Chapter 5 presents the findings of this research work, with sections detailing the performance of the techniques. In this chapter, the results of the experimental implementation are evaluated and discussed to enumerate achievements and challenges encountered during the experimentation process. Chapter 6 concludes the work presented in this thesis and highlights current research directions that are being looked into for future research. The consequences of the findings of this work are recapped in this chapter as well.

Chapter 2
LITERATURE REVIEW

2.1 Introduction

This chapter identifies and evaluates several skin lesion image segmentation and classification reports. To address the image segmentation problem, several algorithms have been put forward by many researchers. These algorithms are broadly categorized as edge-based, thresholding, region-based, and machine-learning-based. Section 2.2 discusses several studies that deal with noise removal from lesion images. This section discusses the various evaluation metrics used for multiple algorithms. Section 2.3 advances an overview of studies on image segmentation in general. This section also discusses the various evaluation criteria and datasets used to test algorithms.

2.2 Overview of previous work related to noise removal from lesion images

To explain the various works in dermoscopic image processing, image segmentation, and the classification of skin lesions, it is necessary first to define the import and significance of the image segmentation process in the skin lesion identification process. The segregation of an image into homogeneous sections pertaining to a specific property such as color, texture, or luminance is referred to as segmentation (Senthilkumaran & Rajesh, 2009). Image analysis is enhanced by segmented images, highlighting previously undiscovered features of the original image. In detecting skin diseases from dermoscopic images, segmentation separates the region of interest (the lesion area) from the background (normal looking healthy skin). Relevant feature extraction, accurate lesion classification, and, as a result, precise diagnosis are all outcomes of effective lesion segmentation (Eltayef et al., 2017). The performance of the segmentation process has a significant impact on the final results of skin disease detection (Mishra & Celebi, 2016).

Sengupta et al., (2019) propose a method that uses median filtering to remove noise from 10 different types of original medical images and Sobel edge detection to segment the section of concern from the image. The authors used entropy as a performance measurement metric. If an image has a higher entropy value after filtration and segmentation, it can be concluded that the image's sharpness has improved.

The authors concluded by emphasizing that their work improved the visualization (noise removal) of medical images and suggested that it be used to help dermatologists identify and diagnose skin lesions. Due to unwanted elements such as light reflection, etc., analyzing skin images captured by digital cameras is a difficult task. This analysis aims to use deep learning techniques to extract the region of a lesion accurately. The authors, Alyari and Jafari Navimipour (2018) propose enhancing camera images with a guided filter to reduce the effects of undesirable elements.

Each image pixel is used as the center of a patch with global and local nature and is fed into a Convoluted Neural Network (CNN). The CNN output is a label for the patch's center pixel. The proposed filter and CNN structure are excellent choices for the segmentation procedure. This experiment used skin images from the Dermquest database with segmentation ground truth. The data was divided into four sections with a train test ratio of 75% to 25%. The experiment's success was determined by its sensitivity, specificity, and accuracy.

In comparison to the L-SRM, Otsu-R, Otsu-RGB, and Otsu-PCA, each of these metrics had relatively high values. However, the proposed methods outperformed the TDLS algorithm on all three-evaluation metrics. Bi, Kim, Ahn, and Feng (2017) proposed a new method based on Image-wise Supervised Learning (ISL) and Multi-scale Super-pixel based Cellular Automata (MSCA) for automatic skin lesion segmentation to address the issue of over or under segmentation of lesions from low contrast images.

First, the hair removal algorithm presented by Lee et al. (1997) is used to eliminate noticeable hair in images. An input image is segmented into a small super pixel by linear spectral clustering. The authors use Cellular Automata Based Segmentation, and to compute the concluding lesion segmentation, across all different scales, integrated the probabilistic maps using a weighted average to achieve pixel-level probabilities.

Some authors have also developed techniques that avoid image preprocessing steps over the years, with remarkable results. One example is a new segmentation approach based on full resolution convolutional networks (FrCN). The suggested FrCN approach learns the full resolution properties of each pixel in the input data directly, removing the need for pre- or postprocessing procedures like artefact removal, poor contrast correction, or further improvement of the segmented skin lesion borders.

The IEEE International Symposium on Biomedical Imaging (ISBI) 2017 and PH2 datasets were used in this experiment. To assess the proposed technique, the paper compares the quality of segmentation to recent methods of deep learning segmentation, such as the Fully Convolutional Network (FCN), U-Net, and SegNet. For the 2017 ISBI sample dataset, the suggested FrCN technique segmented skin lesions with an average Jaccard index of 77.11% and a total segmentation accuracy of 94.03%, 84.79%, and 95.08%, respectively. (Al-masni et al., 2018).

ASLM is a fully automatic region-based image segmentation method for processing dermoscopic images in the presence of obstacles such as oil bulbs, hairs, and reflections. ASLM is computationally efficient and requires no training (Codella et al., 2018). To ensure the successful implementation of ASLM, unwanted artefacts are removed first, followed by skin detection before lesion segmentation, the output of which is two images comprising the detected lesion.

Finally, a binary mask is created by combining the two segmentation images to establish a precise separation between the lesion region and the healthy skin. In this study, the PH2 dataset was used, and the method's success was measured by specificity, sensitivity, precision, and F-measure, which provided 87.1%, 93.5%, 93.6%, and 93.5%, respectively, indicating high performance. The method was also tested against KNN, Bayes, Adaboost, and Random Tree classifiers, yielding excellent results. According to their tests on commercial CPUs, the runtime performance was exceptional.

2.3 Previous Works Related to Lesion Segmentation

The morphology of the lesion's boundaries is an indicator for estimating the presence of skin disease in the analysis of dermoscopic images. Many techniques for segmenting regions of interest from background skin in lesion images have thus been proposed to assist dermatologists in the final clinical diagnostic process properly. This section evaluates and reviews various techniques on skin lesion images to extricate affected lesion areas, employing both semi and fully automatic algorithms.

Chakraborty et al., (2017) proposed a method based on an artificial neural network supported by meta-heuristics to classify skin diseases from digital images in a ground-breaking study. This study looks at three diseases: angioma, lentigo simplex and basal cell carcinoma. When

diagnosing skin diseases, the technique is proposed as a possible solution to decrease the errors associated with diagnosis and surpass the bias of human understanding.

The proposed method trains neural networks for use in skin lesions classification using the Non-dominated Sorting Genetic Algorithm - II (NSGA II). The network was trained using images from the ISIC 2017 challenge. The objective function for single-objective optimization is Root Mean Square Error (RMSE), and for multi-objective optimization, maximum error RMSE is used. The proposed model was compared to two other popular meta-heuristic-based classifiers, NN-PSO (ANN trained with Particle Swarm Optimization) and NN-GA (ANN trained with Genetic algorithm).

The classifiers' performance is evaluated with a confusion matrix-based performance evaluation method. Based on the results, the authors resolved that the NSGA II trained ANN outperforms the other available methods with 87.92% accuracy. Using the same approach on a more extensive training data set could result in a more accurate predictive model. Another group of authors describes a novel technique for automatically segmenting and classifying skin lesions. Experiments were carried out on a private dataset of 726 lesion samples from 5 different types of skin diseases. Their method entails initial segmentation of lesions using a region growing method, feature extraction, and classification using SVM, KNN, and a fusion of SVM and KNN.

The performance measures used to evaluate their technique revealed that their SVNKNN combined classifier outperformed the independent classifiers. They concluded, however, that their proposed technique is suitable for use as an adjunct tool in the diagnosis of skin diseases. The authors believe that using other feature selection methods will help them improve their system. They also intended to improve classification results in the future by experimenting with ANN and PNN classifiers (Sumithra et al., 2015).

Yu et al. (2017) proposes a new technique for detecting melanoma that uses very deep convolutional neural networks (CNNs). To take full advantage of the very deep networks, the authors propose a set of schemes to ensure efficient training and learning with limitations on training data. Residual learning is first applied to solve overfitting and degradation issues as the depth of the network increases. Then, a Fully Convolutional Residual Network (FCRN) is developed for precise skin lesion segmentation. This is further enhanced by including a multi-scale contextual information integration scheme.

Lastly, other extremely deep residual networks are combined with the proposed FCRN to create a two-step structure. Experiments were carried out in ISBI 2016 dataset to determine the efficacy of the proposed method (Yu et al., 2017). Another academic paper presented an utterly automated technique for skin lesion segmentation using 19-layer deep convolutional neural networks that are end-to-end trained and do not rely on previous data knowledge.

In addition, to remove the requirement for sample re-weighting, a unique loss function based on Jaccard distance was developed. In the case where the foreground and background pixels are unbalanced, the technique eliminates the need for rebalancing by directly maximizing the foreground of the ground truth and the foreground of the predicted segmentation mask's overlap. The ISBI 2016 dataset and the PH2 database were used to evaluate the proposed method for effectiveness, efficiency, and generalizability.

The results of experiments indicate that the proposed method performed better than other state-of-the-art algorithms on these two databases. The paper presented relevant details of the method proposed by Yuan et al. (2017) in the design and experiment processes. Zhao et al. (2021) presented a newer approach to skin lesion segmentation in dermoscopic images that is based on a deformable model. The RGB color space is converted in their novel approach to ensure that normal skin and braised skin can be efficiently distinguished based on the information obtained from the image.

The speed function is defined based on color formation lightness and saturation with respect to combining the different color channels and the deformable model's halting criterion. The novel model's performance was evaluated using two image databases. One database contains 90 dermoscopic images, 23 diagnosed as melanomas and the remaining 67 as benign nevi.

The second database, PH2, contained 8 melanoma images and the remaining 152 images as either typical or atypical nevi. With its robustness against noise and flexible segmentation, the proposed method performs better than previously presented algorithms in a quantitative analysis of 250 dermoscopic images. With the current version of this method the initial curves must be manually defined to prevent negative influence from the composite imaging background, thus making it semiautomatic (Ma & Tavares, 2016). Another study proposes a multi-task deep neural network for skin lesion evaluation.

The proposed multi-task DCNN method allows separate sections to share detected features across attribute categories. These components create attribute-specific feature representations,

which are then utilized to infer the attributes via multi-task training on the features. This allowed for the accurate detection of a skin lesion in a dermoscopic dataset. The ISIC 2017 Challenge provided the training and evaluation datasets for this experiment.

The Jaccard Index was used to evaluate segmentation results, and the Area Under the Curve (AUC) was used to evaluate classification results. The multi-task network is also compared to standard DCNN, U-Net for lesion segmentation and GoogleNet for lesion disease classification. All deep learning models in this study were trained and evaluated using 5-fold cross-validation. Compared to individual U-Net and GoogleNet models, the proposed multi-task deep learning model achieves slightly better segmentation and classification performance (Yang et al., 2017).

In some cases, illumination can act as image noise. This creates a situation where the excess illumination must be corrected for the lesion image to be correctly segmented for subsequent classification. Sabouri & Gholamhosseini (2016) propose an alternative to using step-by-step algorithms in detecting lesion borders on skin. They argue that step-by-step algorithms fail when certain image conditions are not met, such as lesion types (which vary greatly), skin color, lighting conditions, and viewing angles.

The paper's authors propose using a Convolutional Neural Network to detect skin lesions by taking an input image of the skin and assigning significance (learnable weights and biases) to different aspects of the image. Using a Convolutional Neural Network was positive, with lesions correctly detected in each image. However, differences in the sizes of the detected lesion borders could be seen. This was because a larger size filter was used to train the Convolutional Neural Network.

A post-processing algorithm was used to smooth the lesion's border to solve this problem. Depending on histogram analysis of the saturation color component in the hue-saturation-value (HSV) color space, a new approach to histogram thresholding for comprehensive segmentation of skin lesions is proposed. The proposed technique is explicitly designed to handle the features' complex variability in macroscopic colored images captured in uncontrolled environments. The proposed technique uses histogram and Otsu thresholding to segment images into mutually exclusive regions.

The evaluation of the method is done using a dataset of 40 macroscopic images containing 30 benign melanoma cases and 10 malignant melanoma cases. The Dice Similarity Coefficient (DICE), false-positive rate (FPR) and true detection rate (TDR) were used to calculate a similarity index between automatically and manually segmented images. The proposed method is unique because it only uses the saturation component of the image's HSV representation (Pirnog et al., 2015).

In their paper, Hassan et al. (2017) proposes a novel segmentation algorithm founded on the Grey Level Co-occurrence Matrix (GLCM). The proposed algorithm does not include any iterative methods or require calibration procedures for the image acquisition system. Their experiments show that GLCM successfully extracted the lesion based on its texture descriptors. The contrast enhancement technique, size, and type of smoothing filter all influence the optimal number of classes. The proposed method's segmentation masks were compared to the human-expert extracted ground truth. The proposed method achieved 98.62% specificity, 96.25% precision, and 80.8% sensitivity.

An innovative region-based segmentation method presented by Mukherjee & Acton (2015) in their paper claims to be capable of segmenting elements even with significant variation in image intensity. The authors report that prevalent solutions for the image segmentation problem employed a type of localized processing to solve intra-region inhomogeneity, which made techniques susceptible to local minima. Therefore, the authors use a set of pre-defined basis functions to represent the illuminated regions of interest in low-dimensional subspaces. The original Chan & Vese (2001) method is generalized because their approach gives room for heterogeneous objects in their proposed method, even in the presence of noise.

The study employs the highest degree of three 1-D Legendre polynomials for region intensity approximation. A dataset of 32 images was used, including a set of faux images with induced noise and simulated intensity and inhomogeneity. The CREASEG tool is used to compare performance to Chan and Vese's algorithm. The proposed method makes it simple to incorporate a priori shape information, which improves performance in some cases. The authors conclude the overall robustness of their formulation. The paper by Yuan (2017) addresses the difficulty in segmenting skin lesions in dermoscopic images due to undesired artefacts, fuzzy borders of lesions, skin texture, and color contrast. The authors present a framework for skin lesion image segmentation built on a deep fully convolutional-deconvolutional neural network

(CDNN). The authors created and subsequently trained a convolutional neural network (CNN) to map from an input image to a posterior probability map.

The neural network comprises 29 layers and has 5 million trainable parameters. The sigmoid function is used as the activation function for the output layer. Principally, CDNN is used as a filter by projecting the entire input image to identify where every element indicates the possibility that the equivalent input pixel is that of a tumor. To reduce the internal covariate shift, batch normalization was applied to the output of each convolutional/deconvolutional layer.

In their paper, authors Romero Lopez et al. (2017) presented a novel deep learning-based approach to classifying a skin lesion as malignant or benign from dermoscopic images. The authors' proposed solution was based on the VGGNet convolutional neural network architecture and used the transfer learning paradigm. The proposed method was designed, implemented, and tested against the publicly available ISIC Archive dataset, yielding impressive results. The method uses an existing CNN architecture developed by the University of Oxford's Visual Geometry Group known as the Very Deep Convolutional Network for Large-Scale Visual Recognition (Simonyan & Zisserman, 2015).

The authors proposed and compared three variations of their method based on the modified VGG16 ConvNet. The first variation involved training the ConvNet from scratch, the second involved using transfer learning to leverage features from a pre-trained VGG16 on a larger dataset. The third variation involved abandoning the transfer learning paradigm and fine-tuning the method ConvNet's architecture. The authors consider loss, sensitivity, precision, specificity, and accuracy as evaluation metrics. The third variation outperformed the current leader with a sensitivity score of 78.66% compared to 50.7%. Their precision value of 79.74% was also higher than the current best result, which was 63.7%. Sensitivity of 78.66% and specificity of 84.00% are good indicators of the quality of the proposed model's predictions.

Yuan et al. (2017) propose using deep convolutional networks to assist dermatologists and improve skin cancer diagnosing accuracy. They used a convolutional-deconvolutional network, which comprises both convolutional and deconvolutional layers. It coaches the datasets from scratch using a convolutional neural network. The ImageNet dataset was used, along with the VGG-16 for good standardization. It divides the primary downside into melanocytic tumors and non-melanocytic (keratin) tumors.

The benchmark datasets were derived from the ISBI 2017 Challenge, including 2000 binary mask images. The Kaiming technique was combined with the simple ConvNet design technique. The VGG16 exploitation transfer learning technique was used as the second technique. The criteria used to evaluate the experiment's performance are Accuracy, AUC, Precision, Sensitivity, and Specification. However, due to the criteria for analysis, the primary technique yielded 51.5%, 73.9%, 37.0%, 86.9%, 44.2% respectively, and thus the second technique yielded 83.7%, 81.6%, 56.1%, 49.3%, 91.3% respectively.

The fully convolutional neural network is used in conjunction with the recently planned fusing layer with a concatenation operation to combine multi-scale discourse information. The dataset for the process was obtained from the ISBI 2017 Skin Lesion Analysis Towards Skin Cancer Detection Challenge. This resolution is implemented in the paper using MATLAB's ASCII text file deep learning tool case "MatConvNet". The analysis metrics were sensitivity, specificity, accuracy, the Jaccard index, and the Dice constant. This experiment's data set includes 150 validation images, 600 test images, and 2000 training images. The ground truth binary mask images from professional manual segmentation are provided with peel values 255 and zero, respectively, indicating lesion peel and skin peel (Qi et al., 2017).

Kawahara et al. (2016) conducted an experiment to demonstrate how pre-trained Convolutional neural networks (CNN) filters generalize to identify 10 groups of non-dermoscopic skin images, outperforming previously published tests. AlexNet's pretrained architecture of ImageNet's natural images was used to build photo features. It was later converted into convolutional layers, with the weights acting as a convolutional filter. With more significant inputs, such filters are then modified to produce responses at different scales. The success of this method is based on avoiding lesion segmentation and complex preprocessing because these are non-trivial steps where errors can propagate (i.e., poor segmentations can give poor characteristics). The dataset for this study is Dermofit Photo Library.

The use of subtracted images per object, mean pooled-multi-scale feature extraction, and pooling via augmented feature space resulted in significant improvements in classification accuracy. Li & Shen (2018) proposed two deep learning systems, the Lesion Indexing Network (LIN) and the Lesion Feature Network (LFN), in this study to solve three major challenges of skin lesion image processing: lesion segmentation, dermoscopic feature extraction, and lesion classification.

The Lesion Indexing Network was created to address lesion segmentation and identification simultaneously. Two very deep, completely convolutional residual networks with different training sets were used to produce the segmentation and coarse classification results. To identify lesions, it is proposed that a lesion indexing unit (LICU) be used to determine the value of a pixel. The coarse category's product is refined using LICU's distance map. The Lesion Feature Network is a CNN-based system trained on patches extracted from dermoscopic images to address the task of dermoscopic feature extraction. The ISIC 2017 dataset was used in this study. Lesion Indexing Network's JAC and AUC for lesion segmentation and classification are 0.753 and 0.912, respectively, outperforming existing deep learning frameworks at the time.

The proposed LFN achieves the highest average accuracy and sensitivity for dermoscopic feature extraction, 0.422 and 0.693, respectively, demonstrating its superior ability to meet the challenge. Sarker et al. (2018) attempt the significant task of self-operating melanoma diagnosis in Skin Lesion Segmentation in dermoscopic images. A CAD system is required to assist dermatologists in effectively analyzing dermoscopic images and meticulously segmenting melanomas. Nonetheless, this task remains difficult because dermoscopic images have a variety of characteristics.

Convolutional Neural Networks derived from encoder-decoder networks and other modern deep learning methods applied to image analysis have been used to solve the image segmentation problem. The first layer in the encoding phase is a 3 x 3 convolutional layer, followed by a 3 x 3 max-pooling with stride 2.0 that generates 64 feature maps. Diversely, for the decoder network, the concept of PPN is used to create multi-scale feature maps, which are then strung together to produce more robust feature maps. In this study, the ISBI 2016 and ISBI 2017 datasets were used to evaluate segmentation performances such as Specificity, Sensitivity, Jaccard index, Dice coefficient, and Accuracy, with the SLSDeep producing the best results. Compared to other methods such as ExB and CUMED, the SLSDeep had results with an overall accuracy of more than 98%, indicating that the SLSDeep properly segmented the lesion area with accurate sharp edges.

Another experiment by Nasir et al. (2018) proposed a new CAD model approach to assist dermatologists in more accurately diagnosing melanoma. This method identifies and classifies melanoma significantly better than previous methods. The proposed system started with pre-processing operations and then used the effective contour approach to segment the lesion region by fusing new uniform distribution segmentation. In the feature extraction step, three features

are merged: color, texture (SFTA), and HOG, and then the maximum entropy-based selection is made. The tests were performed on a publicly available PH2 data set. The results are based on various feature combinations and feature and classifier selection methods.

The authors Perez et al. (2018) studied the effects of thirteen scenarios of data augmentation for the classification of skin melanoma trained on ResNet, DenseNet and Inception-v4, which are Convolutional Neural Network Architectures. The scenarios considered by the authors include the conventional color and geometric transforms, as well as uncommon augmentations such as random erasing and elastic transforms. The authors also examined the application of data augmentation techniques during testing and their effects on various dataset sizes. For the skin melanoma classification task, the experiments were carried out on the dataset provided by the 2017 ISIC challenge.

The results of various data augmentation scenarios with different image processing techniques are presented. The results showed that the Inception-v4 architecture for the training with 500 images coupled with data augmentation outperformed training using the same architecture but on 100, 1500 and 2000 images without augmentation. With 1000 images and data augmentation, ResNet and DenseNet achieved a higher AUC than with 1500 and 2000 images without augmentation. The findings support the relevance of data augmentation at both the training and testing phases. It also demonstrates the potential to result in more incredible performance gains instead of obtaining new images.

The scenario with optimum performance yielded an AUC value of 0.882 for melanoma classification without the use of external data. This outperformed the topmost rank submission of 0.874 AUC value for the 207 ISIC challenge, which was carried out with additional data. A novel convolutional neural network (CNN) architecture is proposed in this paper by Kawahara et al. (2016) to classify different types of skin lesions by learning from multiple image resolutions while leveraging pre-trained CNNs. This proposed CNN analyzes the image at multiple resolutions at the same time using multiple tracts, and interactions across numerous image resolutions using the same field of view are learned.

A CNN that has been trained on a single resolution is converted to work with multi-resolution input. When given a skin lesion image x, it predicts the true lesion class label y. The proposed method was tested using the Dermofit Image Library. The proposed system was found to

improve classification accuracy. The validity was approximately 0.781, compared to approximately 0.674 for existing methods.

This paper proposes an automatic analysis of dermoscopic images (Bi, Kim, Ahn, Feng, et al., 2017). Deep residual networks (ResNets) can analyze complex images to learn and represent visual features. The lesion is segmented using the fully convolutional network architecture, including convolutional and deconvolutional layers. After that, the lesions are classified into various diagnoses, including melanoma. The proposed segmentation method (ResNet-Seg) was compared to the FCN architecture (VGGNet model). The averaged area under the curve (AUC) was used for the evaluation, yielding 84.3, 85.5, and 85.4 for the multi-class, binary, and ensembled ResNet, respectively.

The datasets ISIC and ImageNet were used. Image processing techniques and mobile technologies are used in another paper by Joseph & Panicker (2017) for a non-invasive automated skin lesion analysis system for the early detection of melanoma. Hair follicles are detected and removed from images for effective classification, and skin wound features are extracted. The proposed method is based on a 2D Gaussian derivative and a fast marching in-painting algorithm. A careful examination of the skin's features enabled the decision to be made about whether a skin cancer test was required. The system was created using MATLAB. In summary, the system detects hair, segments the lesion, extracts features, and determines whether the lesion is malignant or not. PH2 is a dataset obtained from Pedro Hispano Hospital.

Sensitivity, specificity, and accuracy were all determined. When given some random inputs, the first classifier produced 93%, 90%, and 91.5% for sensitivity, specificity, and overall accuracy, while the second classifier produced 95%, 92%, and 93.5%. U-Net, a deep learning technique, is used to improve deep learning-based semantic segmentation methods. A Recurrent Convolutional Neural Network (RCNN) based on U-Net is proposed, and a Recurrent Residual Convolutional Network (RRCN) based on U-Net models, namely RU-Net and R2U-Net. The advantages of this approach include: a residual unit that aids in deep learning architecture training; and better feature representation for segmentation tasks through feature accumulation with recurrent residual convolutional layers.

A better U-Net architecture with the same network parameters and improved performance for medical image segmentation can also be designed. The proposed models were tested in medical imaging applications such as retina blood vessel segmentation, skin cancer lesion segmentation,

and lung segmentation. Compared to existing methods such as U-Net and Residual U-Net, RU-Net and R2U-Net outperformed them on all datasets. STARE, CHASE DB, and DRIVE data sets were used. The models were evaluated using SE, SP, JSC, F1-Score, AC, and AUC, with R2U-Net producing 0.9832, 0.944, 0.9918, 0.9823, 0.9918, and 0.9889, respectively (Alom et al., 2018).

The following proposed method incorporates preprocessing, lesion segmentation, feature extraction, feature selection, and classification (Nasir et al., 2018). In the preprocessing stage, DullRazor removes hair and lesion texture, and color information is used to improve lesion contrast. A hybrid technique is used for segmentation, and the additive law of probability is used to fuse the results. Then, a serial-based method is used to extract and fuse traits like color, texture, and HOG (shape). The fused features are chosen using a novel Boltzmann Entropy method. Finally, the Support Vector Machine (SVM) classifies the selected features. The proposed method was evaluated using the publicly available PH2 dataset.

The evaluation metrics were sensitivity, specificity, accuracy, and F1-Score, which yielded 97.7%, 96.7%, 97.5%, and 97.5%, respectively. When tested on the same dataset, existing methods did not produce such good results.

2.4 Conclusion

This chapter discusses a survey of the current state-of-the-art design and implementation of skin lesion segmentation and classification systems. The chapter reviews explicitly efforts made by other researchers in the field of noise removal in dermoscopic images. The leading methods for the segmentation of dermoscopy images for the detection, classification and diagnosis of melanoma are highlighted in this chapter. The subsequent chapters delve into the focus of this thesis, the evaluation of noise removal schemes and their relevance to the segmentation process.

Chapter 3
METHODOLOGY

3.1 Introduction

Different machine learning technologies are employed for computer-assisted diagnosis of melanoma detection and malignancy classification. The introduction to this chapter gives a brief overview of these technologies. Here, introductions to major machine learning concepts are highlighted to put the scope of the study in perspective. Section 3.2 presents an overview of machine learning concepts and categorizations of machine learning algorithms. Section 3.3 highlights leading hair removal techniques, advantages, and drawbacks. Further analysis of the mathematical foundations of some of the presented hair removal algorithms is also presented.

3.2 Overview of Machine Learning

Machine Learning (ML) is a branch or field in the Artificial Intelligence (AI) discipline that focuses on developing applications that learn from data and improve their accuracy over time without being taught to do so. Machine learning aims to create new algorithms based on given data to make predictions. Using training data, ML algorithms generate general models so that these models can detect the existence or lack of a pattern in new (test) data. Training data may be in the form of pictures, regions, or pixels that are labelled or otherwise, in the case of this thesis images are the focus. Patterns may be low- level or high-level. For example, a low-level pattern can be a tag for pixels in segmentation, whereas the presence or absence of a disease in a medical image can be a high-level pattern. In this case, with a training set containing image label pairs, the image classification becomes the problem solved.

3.2.1. Machine Learning Algorithm Classifications

Based on various learning issues, machine learning techniques or algorithms can be separated into three main groups. The categories are as follows:

- Supervised Learning: In supervised learning, the dataset for training must be in a specific format, and each instance is assigned a label. Datasets are labelled as $(x, y) \in X \times Y$ where x and y represent a data point and the corresponding true prediction for x.

The learning problem is considered a classification task if the output y is part of a discrete domain. It is a regression task if the output belongs to a continuous domain.

- Unsupervised Learning: Unlike supervised learning, the datasets in unsupervised learning are not labelled. The ML algorithm should analyze the similarities between object pairs to create a structure from unlabeled data.
- Semi-supervised Learning: This learning task is a supervised learning task that uses a high volume of unlabeled data and a limited amount of labelled data for preparation.

3.2.2. Neural Networks

A significant component of the human brain is the biological neural network. It is a highly dynamic system that can simultaneously process multiple tasks. A classifier that simulates the human brain and neurons is the neural network (NN). As the simplest unit of NN, "perceptron" is used instead of neurons. (See Figure 3.1).

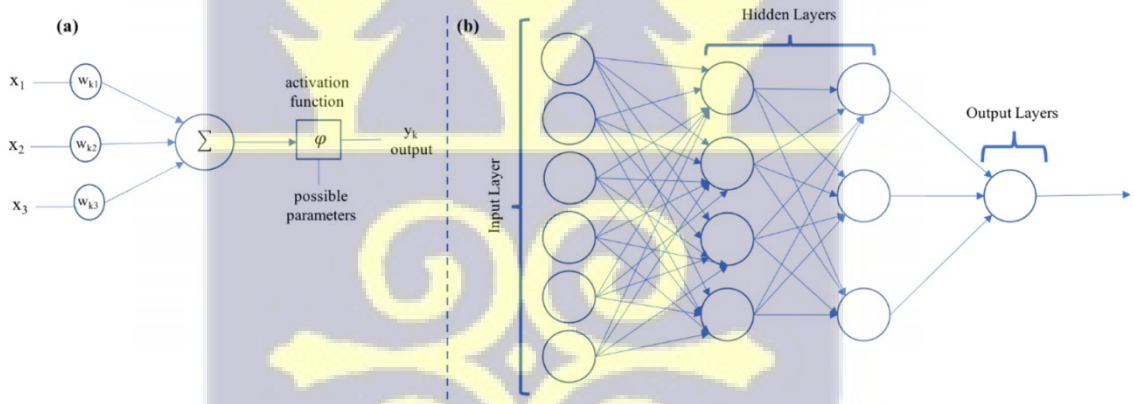

Figure 3.1(a) is the perceptron layer and (b) is the image of Multi-layer Neural Network

As displayed in figure 1 above, the NN architecture comprises different layers:

1. the input layer containing the vector(s) input function
2. The output layer contains the neural network response, and
3. The layer contains the neurons (perceptron) between the input and output layers.

According to the McCulloch-Pitts model by Chakraverty et al. (2019), the input parameter X_j is received by neuron k. A weight parameter (W_{kj})is also present in the neuron. The sum of inputs and weights is combined and fed into an activation function φ which produces the output

y_k of the neuron as seen in Figure 3.1(a). Equation (3.1) below explains neural networks mathematically.

$$Y_k = \varphi \sum_{j}^{m} W_{kj} X_j \tag{3.1}$$

By choosing the weights of all neurons, a neural network can learn the approximate target outputs after training. Analytically solving neuron weights of a multi-layer network, however, is difficult. The back-propagation algorithm is used to resolve the weights iteratively in a simple and efficient manner.

3.2.3. Convolutional Neural Networks

A convolutional neural network (CNN) is the most popular artificial neural network used in computer vision. CNN's are used in computer vision problems for two essential purposes. Solving the computer vision problem with conventional NNs is difficult even for relatively small pictures. Compared to other image classification algorithms, CNNs need very little image pre-processing, which means CNNs can learn the filters independently. The input and output layers, as well as the various hidden layers, make up the CNN. Convolutional layers are completely linked layers, and pooling layers are commonly used in the hidden layers. In figure 2 see an example of a convolutional neural network. Convolutional Layers: These layers transfer the previous layer's output to the subsequent layer. It mimics a neuron's response to visual input. Pooling Layers: These layers merge the outputs of a layer's neuron clusters into a single neuron in the next layer. The objective of this layer is to minimize the network's parameters and computation. Fully-connected layers: These layers link every neuron in one layer to every neuron in the next layer (Thoma, 2017).

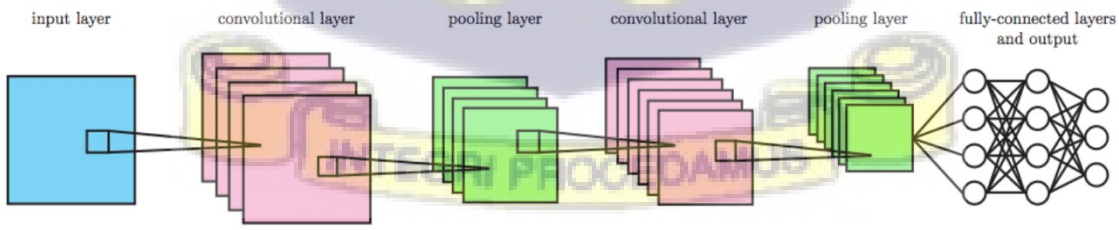

Figure 3.2: An example of a convolutional neural network. Image credit: (Münker & Stenroos, 2017)

3.2.4. Deep Learning

Deep learning, often referred to as Deep Structured Learning, is a subcategory of machine learning that employs a variety of algorithms. Since most current deep learning models are built on NN, deep learning has a cascade of multiple layers similar to NNs. Deep learning differs from traditional machine learning techniques in that it can derive relevant attributes directly from multiple sources of data including images, sound, and text in supervised and/or unsupervised ways. In reality, feature extraction is considered a step of the multistep learning process when working with this method. These characteristics of deep learning results in the diminished necessity for hand-tuned machine learning methods in modern day problem solving.

3.3 Dermoscopy Image Hair Removal Techniques

Dermoscopy image hair and hair-like regions inside skin lesion images must be removed and restored for features within lesions to be more effectively assessed for disease identification and diagnosis. A few procedures are available in the literature for repairing thin and thick hair. These investigations are primarily concerned with the hair detection error, with the impact on tumor patterns often being overlooked. Consequently, this removal of hair treatments frequently results in undesired blurring, disrupting the tumor's texture, and color bleeding. Furthermore, these techniques tend to be computationally expensive. Linear interpolation approaches, inpainting by nonlinear partial differential equation-based diffusion algorithms, and exemplar-based methods are all examples of hair removal methods. The following sections examine these strategies in further depth.

3.3.1 Nonlinear PDE-based diffusion techniques for hair removal

This is an unsupervised learning-based repair algorithm for eliminating hair from images of skin lesions before segmenting and analyzing malignant melanoma. Most often, the hair occludes important information on the skin image and this algorithm is employed to correct that. This technique usually comprises three (3) major steps, namely, Enhancement & segmentation of the melanoma image, secondly extraction of the hairs from the segmented image. After these processes, the third step is the in-painting of the image using the non-linear PDE-based diffusion method. They work convincingly well as image restoration algorithms and thus may not be holistically suited for the task at hand (thus, image enhancement). In

practice, the nonlinear PDE-based diffusion method is essential to identify the boundaries of tumors due to its capacity to preserve edges. Non-linear-PDE diffusion schemes are popularly used as a preprocessing step before lesion detection (Marchetti et al., 2018). Inpainting, the process of restoring the fundamentals of visual artifacts, involves the completion of unknown data points in a known region of an image with the primary objective of harmony restoration to deprecated images that have been worn down over a period or objects that we desire to remove from an image. Inpainting methods that are used currently are either Partial Differential Equations (**PDE**) or Total Variation Equation (**TVE**) based. For small scale target restoration, PDE-based methods have a superior property of maintaining the image's linear geometry feature by visualizing information diffusion through the difference in pixels. Since hair objects can be viewed as small objects in small areas, PDE algorithms are suitable to be used on them. The three main steps involved in non-linear PDE-based diffusion methods are further elaborated as follows.

- **Enhancement and Segmentation:** Hairs in an image can easily be detected, as hairs are a kind of curved object. There are several methods for curved objects such as Least Squares Method (LSM), both standard and randomized Hough transform among others. These techniques are primarily used to detect curve objects with known models; however, they are ineffective for curve objects with unknown models or cross each other such as hairs. A suitable strategy for detecting hair curves is to enhance the image using a morphological closing-based top-hat operator, after which a binary image is generated threshold techniques based on probabilities. The hairs are then isolated from the background skin. The morphological top-hat operator is a basic toolbox of mathematical morphology operators for grayscale imagery. The top-hat operator is commonly used to detect objects against backgrounds that aren't uniform. The top-hat operator has two different versions for grayscale images. These are the opening and closing top-hat operators responsible for extracting bright and dark structures from images, respectively. The closing top hat operator may enhance hair objects on a grayscale image since the pixels inside the hair are darker than the ones surrounding it, allowing them to be considered black structures. Enhanced hairs form the image's bright regions, and the space of these bright regions takes up a certain proportion of the overall image. The improved image is then subjected to threshold segmentation.

- **Hair Extraction:** Non-hair noise is often identified with hairs, with hair connected areas being larger and longer than the connected regions with no hair, which are smaller and shorter. It's easier to extract hairs from an image by measuring the surface area of the connected region. However, a portion of the hair that is short is likely to get lost in the large, connected regions with no hair.

  In one approach, each pixel in the specified hair region is checked to see if the hair is enclosed within a thin and long structure; if it isn't, it is discarded as noise. Up, down, left, right, and the four diagonals are the eight directions in which line segments are drawn from the pixel until they reach regions with no hair. Four straight lines with the pixel in the middle are created from the eight-line segments. The line with the greatest length is identified after the lengths of all the lines have been computed. The largest line must be at least 50 pixels long, while all other lines must be under 10 pixels long. Otherwise, the pixel is also rejected if it isn't a hair pixel. This hair extraction metric is only based on pixels and ignores the relation between pixels in the same hair area. Another method extracts the hairs from the image by measuring the length of connected regions. The ratio of the short axis to the major axis is used to determine the length of the linked region. The formula is given by equation (3.2).

$$e = \frac{\alpha}{\beta} \tag{3.2}$$

  where e is the elongate, α is the length of the short axis and β is the length of the major axis

- **Image inpainting based on Partial Differential Equation (PDE):** By eliminating the hair regions from further investigations, the impact of hair on diagnostic analysis is eliminated. In the last decade, non-linear diffusion filters have been widely used in edge preservation and enhancement filtering (Abbas et al., 2011). The gray levels of an image (U) are diffused according to equation (3.3)

$$\frac{\partial u}{\partial t} = div(c(x, y, t)\, \nabla u) \tag{3.3}$$

  with ∇ as the gradient operator and div(.) as the divergence operator.

  Having a coordinate (x, y) of a pixel, the scalar diffusivity $c(x, y)$ is chosen as a decreasing function $g(\cdot)$ of the gradient ∇U. This controls the operations of the diffusion process. An obvious option for diffusivity function is shown mathematically in equation (3.4).

$$c(x,y,t) = g(\nabla U) = \frac{1}{1 + \left({}^{\nabla U}/_{K}\right)^2} \tag{3.4}$$

With *K* being *the* gradient threshold. Impressive results are obtained from the practical implementations of the P-M filter. Image noise is removed, and edges are preserved and possibly made better if their gradient value is larger than *K*.

The following equation is a partial differential equation that is anisotropic in nature, let $u_1(x, y)$ be the original image, then the discrete iterating form of the equation for image inpainting is equation (3.5).

$$u^{t+1}(x,y) = u^t(x,y) + \frac{\lambda}{n} \sum_{Q \subset D} c\big(\nabla^t u(x,y)\big) \nabla u^t(x,y) \tag{3.5}$$

where (*x, y*) is a pixel coordinate, D is the neighborhood of the *(x,y)* pixel, the positive constant λ represents smooth degree, n is the number of neighborhood pixels, *t* is iteration times. The hair sections recovered from images with the elongate measure are used as masks in color images of skin diseases. The inpainting result is generated by iterating equation (3.5) repeatedly inside the region of the mask in three color bands on the original image.

3.3.2 Hair removal by linear interpolation methods: Linear interpolation methods have three main steps: (a) detecting dark hair; (b) replacing hair pixels with adjacent non-hair pixels; and (c) smoothing the final image.

(a) To identify dark hairs, a generalized version of the grayscale morphological closure operation is applied individually to the three-color bands. The grayscale closure operation smooths out the low-intensity values along the structural element direction, i.e., the dense dark hair pixels. Experiments show that three distinct structural components, 0 degrees horizontal, 45 degrees diagonal, and 90 degrees vertical, are suitable for smoothing all dark hairs (Abbas et al., 2011). The generalized grayscale closing image is created from the highest response (in all three directions) of grayscale closing. Finally, the absolute distinction between the generalized grayscale closure picture and the original color band is crossed to generate a binary hair mask image.

The generated hair mask separates the areas with hair and areas without hair. Consider G_7 to be the closing image resulting from the generalized grayscale of the original red band O_7, and S_{81}, $S_{9:}$ and S_1 are the structural elements in the vertical, diagonal and horizontal directions respectfully. Gr, is the expression in equation (3.6).

$$G_r = |O_r - max\{O_r \cdot S_0 \cdot O_r \cdot S_{45} \cdot O_r \cdot S_{90}\}| \quad (3.6)$$

Where the grayscale closing operation is represented in the expression by ·. Additionally, at the location (x, y), $M_7(x, y)$, the binary hair mask pixel is calculated as:

$$M_r(x,y) = \begin{cases} 1, & if\ G_r(x,y) < T \\ 0, & otherwise \end{cases} \quad (3.7)$$

where the predefined threshold value is represented by T in equation (3.7).

We can write a similar expression for both the green and blue bands. The union of each of the masks for the 3 color bands produce a final mask for the original image.

$$M = M_r \cup M_g \cup M_b \quad (3.8)$$

Where M_r, M_g, and M_b, in equation (3.8) are the hair masks for the color bands red, green and blue respectively.

(b)The binary hair mask, derived from the preceding step, is employed to facilitate the replacement of corresponding pixel values of the original image with the nearby non-hair pixel values. Each pixel in the hair region of the mask M is examined before the replacement operation to ensure that it is located within a long and thin structure, that is, the hair structure; otherwise, it is rejected as noise. Line segments are drawn in eight directions, up, down, left, right, and the four diagonals, radiating from each pixel inside M's hair region until the section arrives at the region without hair. The eight-line segments combine to create four straight lines that intersect at the pixel. The lines' lengths are computed, and the longest is recorded. The longest line must be at least 50 pixels long, and all other lines must be less than 10 pixels long. If this is not the case, the pixel will be rejected. When a pixel is proven to be inside the hair structure, it is replaced in the original image by adjacent non-hair pixel values along the shortest line and the line perpendicular to the longest one, using bilinear interpolation. The precise hair border location cannot be determined since the bitonal hair mask, M, is created using the thresholding method mentioned in step a. This is due to the threshold value's imprecision, image noise, and the penumbra effect on the hairs. The interpolation algorithm selects non-hair pixels, 11 pixels away from both sides of the hair borders and along the shortest line segment to overcome the border problem.

Let l(x, y) be the intensity value for the replacing pixel, l_1(x1,y1) and l_2 (x2,y2) be the selected non-hair pixel intensities along the shortest direction. The new intensity value $l_n(x \cdot y)$ can be expressed in equation (3.9):

$$l_n(x \cdot y) = l_2(x_2 \cdot y_2) * \frac{D\big(l(x \cdot y) \cdot l_1(x_1 \cdot y_1)\big)}{D\big(l_1(x_1 \cdot y_1) \cdot l_2(x_2 \cdot y_2)\big)} + l_1(x_1 \cdot y_1) * \frac{D\big(l(x \cdot y) \cdot l_2(x_2 \cdot y_2)\big)}{D\big(l_1(x_1 \cdot y_1) \cdot l_2(x_2 \cdot y_2)\big)} \quad (3.9)$$

(c) Due to the thresholding method, image noise, and the penumbra effect, the exact border locations are difficult to detect in the previous step. To smooth out thin lines formed around the border of the hair regions, an adaptive median operator is used in this step. A new hair mask with slightly bigger hair regions is built using a binary dilation operation with a 5 X 5 square structure element of all *l*'s, centered in the middle of the square. The enlarged hair regions are given a 5 X 5 median filter to retain the finer details, while the non-hair parts are kept intact.

3.3.3 Hair removal method by fast marching scheme

The three steps of this algorithm are hair identification using Gaussian derivatives, refinement using morphological approaches, and restoration using a fast-marching image inpainting technique.

- **Hair detection from dermoscopy images:**

Initial hair-like artefacts segmentation: dermoscopic pictures are used to detect correct lines, and some attributes are determined to separate them from nearby pixels. In addition to direction, these attributes can be described as thickness, magnitude, and length. On the other hand, the properties of the lesion may be recognized since they lack these characteristics. For the difference in thickness lines, the hair line identification approach based on the 2-D derivatives of a Gaussian of the luminance component (L*) of the image in the CIEL*a*b* color space is determined by equation (3.10).

$$R_D(x, y) = g_i(x, y) * i(x, y) + g_\theta(x, y) * i(x, y) \quad (3.10)$$

The input image's L component is $i(x, y)$, * is a convolution operator, while $g_D(x, y)$ and $g_E(x, y)$ is gaussian derivative for thin smooth lines and thick lines detection respectively. Instead of multiplication, a 2-D convolution operator (*) is employed especially because it uses a smoothing function in the x and y directions. The application of L* adapts the method to human discernment since the perceived lightness response of the visual system of humans is

matched by the design of the luminance in the uniform color space. The smooth thin lines detection filter's 2-D Derivative of Gaussian (DOG) is defined by equation (3.11).

$$g_i(x,y) = \frac{-x}{\sqrt{2\pi\sigma^3}} e^{\frac{-x^2}{2a_i^2}}, for\ |x| \le 3\sigma_i, |y| \le \frac{L_i}{2} \tag{3.11}$$

This Gaussian derivative effectively recognizes multi-directional lines. i is the Gaussian function's standard deviation at scale i and Li is the filter's y-direction span. The tangent direction of a line is smoothed with the parameter Li. Then, using $g_D(x,y)$ a rotation with angle is applied (Joseph & Panicker, 2017).

$$g_i^{\theta}(x^i y^i) = g_i(x,y) \tag{3.12}$$

where $x_D = xcos\theta + ysin\theta$ and $y_D = ycos\theta - xsin\theta$ in equation (3.12).

There are also some lines that are substantially thicker than regular ruler markings or hair lines, such as blood vessels. A Gaussian function with weight towards the center of the image is defined in equation (3.13) to attain this characteristic.

$$g_\theta(x,y) = \cos\frac{\pi x^i}{2\alpha}\cos\frac{\pi y^i}{\alpha} e^{-\frac{x^2+y^2}{2(0.5\alpha)^2}} \tag{3.13}$$

where α = 0.5 (a fixed value). The maximal centerline filter is used to determine the line's direction. The distance between a local maximum and a local minimum along the perpendicular direction of the line can be used to estimate the line width. After obtaining the center, the direction and width of the lines are interpolated using data gathered through a thresholding technique. The thresholded approach established by Ridler & Calvard (1978) is iteratively followed to calculate an automatic thresholded value. The technique first computes the image's mean intensity values. Subsequently, the technique computes for the mean intensity values, mean values that are higher and lower using these threshold values. Finally, to determine the threshold value, this technique is employed iteratively. Unwanted curves and parts of the tumor structure can be recognized by calculating these properties.

- **Refinement of hair segmentation lines**

This hair detection approach is used to break weak sections of hair-occluded lines. In an image, all identified lines are scanned. We connect these lines, which are 10 - 20 pixels apart in all eight directions, using the two pixels linking method. The shape or curvature of segmented hairlines was comparable to those of other items. The tumor region or dermoscopic-gel could be the source of these contour-like curves. As a result, the estimated circularity and morphological area opening conditions are applied to obtain hair lines without these contour items. A method devised by Haralick et al. (1973) is used to quantify circularity, which is based on the mean and variance of radial distances. The hair mask is efficiently segregated using this circularity condition. Furthermore, the morphological area-opening feature is employed to ignore undesired little objects. If the undesired items are round and have an area of more than 90 pixels, they are filtered out. Hair segmentation results are produced by deleting undesirable elements from the hair mask.

It is crucial to smooth and fill these lines before inpainting them. Morphological operators (dilation and filling) are applied to a mask image that constrains the transformation and defines the connectivity with a structural element to achieve smooth hair lines. This method uses the 8-pixel connection structural element in all directions. After this structural feature is specified, the binary mask picture is subjected to an image dilation technique. In some of the detected lines, there will be some gaps. As a result, a morphological area-filling function is applied to the dilated mask. The holes in the image that define each line's outline must be filled before applying an area-filling operator.

Let *M(x, y)* denote a dilated binary mask image in equation (3.14), and suppose that the hole filling image P, be 0 everywhere except on the image line's border, where it is set to *(1−M(x,y))*:

$$P(x,y) = \begin{cases} 1 - M(x,y), & if\ (x,y) is\ on\ the\ border\ of\ M \\ 0 & ,otherwise \end{cases} \tag{3.14}$$

Then equation (3.15)

$$HoleMask = \left[R_{M_c}(P)\right]^c \tag{3.15}$$

is a binary filled hair-mask image, where $R_{O(}(P)$ denotes the reconstruction of M(x, y) from P*(x, y)*. In this way the HoleMask *(x, y)* image is obtained along with x and y coordinates. Then, a fast-marching scheme is utilized to inpaint the identified lines.

- **Texture-area restoration of hair-occluded information:**

Two basic elements comprise a fast-marching approach for image inpainting: a. replacing the weighted function (b) boosting the method's reliability by substituting the coherence direction for the edge-oriented transport direction. To choose an adequate weighted function *w (x, y)* for a single pass inpainting technique, the normalized directional dependency *w* is defined by equation (3.16).

$$w(x,y) = \left(\frac{\pi}{2}\right)^{\frac{1}{2}} \mu/|x-y|\, e^{\left(-\frac{\mu^2}{2}\right)}|\, c\,|(x)\,(x-y)|^2 \tag{3.16}$$

This fast-inpainting method has an advantage over others since it uses a directional vector c that is aligned with the level lines (isophotes) of image u. The time variable is stabilized, and edge-directional flow is introduced for faster and more effective inpainting. For these reasons, the integral differential equation was created using a hybrid splitting technique in equations (3.17) and (3.18).

$$u^t(x,y) = -\nabla^{\perp}\nabla_{u_\sigma}(x,y)\nabla u(x,y) \tag{3.17}$$

and

$$u_\sigma(x,y) = k_\sigma u(x,y),\;\; k_\sigma(x) = \frac{1}{2\pi\sigma^2} e^{\left(x\frac{|x|^2}{2\sigma^2}\right)} \tag{3.18}$$

The formal stationary equation of equation (3.17) is given by equation (3.19) as;

$$\pm\, \nabla^{\perp}\nabla_{u_\sigma}(x,y)\nabla u(x,y) = 0 \tag{3.19}$$

While the edge-direction flow is defined with equation (3.20).

$$\vec{c}(x,y) = \nabla^{\perp}\nabla_{u_\sigma}(x,y) \tag{3.20}$$

The direction of coherence is found using a robust structural tensor technique (Brox & Weickert, 2004). As a result, the structure tensor J_T of the image $u(x, y)$ is given by equation (3.21).

$$J_p\left(\nabla_{u_\sigma}(x,y)\right) = k_p\left(\nabla_{u_\sigma}(x,y) \otimes \nabla_{u_\sigma}(x,y)\right) \tag{3.21}$$

Hence, the coherence direction in equation (3.22)

$$\vec{c}(x,y) = \overrightarrow{w_1} \tag{3.22}$$

Where w_1 is the normalized eigenvector to the minimum eigenvalue of J_T i$\nabla_*(x, y)$j at scale p on the second moment. Furthermore, for RGB color space the modified form of the structure tensor for color images is defined as:

$$J^m_{\sigma \cdot p}(u) = 0.299 J^m_{\sigma \cdot p}(u_R) + 0.587 J^m_{\sigma \cdot p}(u_G) + 0.114 J^m_{\sigma \cdot p}(u_B) \quad (3.23)$$

As previously stated, the RGB color space is unrelated to human eyesight. As a result, equation (3.23) is unsuited to human perception and may have undesired effects such as blurring.

To avoid this issue, we use the CIE L*a*b* uniform color space, which improves the structure tensor equation:

$$J^m_{\sigma \cdot p}(u) = 0.412453(u_{a+}) + 0.715160 J^m_{\sigma \cdot p}(u_{a-}) + 0.950227 J^m_{\sigma \cdot p}(u_b) \quad (3.24)$$

As a result, the algorithm achieves a level of adaptation to the human visual system that its previous form did not. Equation (3.24) gets its constant values from the RGB to CIE L*a*b* transform matrix.

3.3.4 Hair removal by exemplar-based in-painting methods

First, a target region is chosen from an input image to be eliminated and filled. The source region can be supplied manually or as the complete image minus the target region (ϕ =I- Ω, as a dilated ring around the target region). Also, $\delta\Omega$ is utilized to represent the target region's boundaries. An exemplar-based inpainting algorithm typically includes the following steps:

- **Initialize the target region:**
  This is usually done separately from inpainting and necessitates the use of a different image processing program. This is accomplished by highlighting the target area with a distinct color. Assume that the target region will be designated in green,
  (i.e., R = 0, G = 255, B = 0) without losing generality.
- **Select a patch from the region to be in-painted:**
  The patch should be larger than the image's most discernible texture component. A default patch size of 9 × 9 is most commonly used, but this can be altered given knowledge of the image's largest texture element. The letter *p* denotes the patch.
- **Find a patch from the image which best matches the selected patch, p:**

A suitable error metric can be used to match the data. To find the best matched patch, the Mean Squared Error in equation (3.25) is used.

$$MSE = \sum \frac{(f_{x,y} - g_{x,y})^2}{N} \tag{3.25}$$

The patch p and the other elements for which MSE is to be computed are $f_{x,y}$ and $g_{x,y}$ respectively. The total number of patch elements is N.

- **According to the patch obtained in the previous step, update the image information:**

The accomplished results are very likely to depend on the order of selection. This has prompted the development of methods that attempt a redefinition of the order of selection to improve results. To successfully select the best section out of the defined target region, a priority function is defined multiplicatively as

$$P(p) = C(p) \times D(p) \tag{3.26}$$

where C(p) is the patch's confidence term and D(p) is the patch's data term respectively from equation (3.26). Equations (3.27) and (3.28) define these terms, respectively.

$$C(p) = \frac{\sum q \in \psi_p \cap \varphi \, C(q)}{|\psi_p|} \tag{3.27}$$

$$D(p) = \frac{\nabla I_p^{\perp} \cdot n_p}{Y} \tag{3.28}$$

where Y is the normalization factor (equal to 255 for a normal grey level image), $I\psi_T|p|$ represents the area of the patch ψ_T and, n_T is a unit vector orthogonal to the front of $\delta\Omega$ at the point p. ∇I_T^Q denotes the isophote perpendicular at point p. The gradient for the source region determines the value n_T.

The source region is a matrix with all ones on points that aren't in the target region and zeros on all other locations. (i.e. for the points in Ω). The gradient of the image can be used to determine the isophote. Cheng et al. (2019) observed an exponential decline in the confidence expression as defined by Criminsi, necessitating the replacement of the multiplicative definition of the priority term. They also claimed that the order of the

data term in the additive form of priority did not match the confidence term. As a result, they used the regularized confidence term for modification. In addition, the authors advocated those different components in the definition of priority terms be given weights to maintain a balance between confidence and data terms. As a result, the amended priority phrase now looks like equation (3.29).

$$P(p) = \alpha \times R_c(p) + \beta \times D(p), 0 \leq \alpha, \beta \leq 1 \tag{3.29}$$

Where α and β are the component weights for the confidence and data terms, respectively. Also, $\alpha+\beta= 1$ and $R_c(p)$ is the regularized confidence term.

$$R_c(p) = (1 - \omega) \times C(p) + \omega, 0 \leq \omega \leq 1 \tag{3.30}$$

Where is the regularizing factor for determining the smoothness of the curve is ω.

Using this confidence term, the value of the confidence term is regularized to [ω,1]. The new priority function will be able to withstand the "*dropping effect*" in this respect. Now that we have the patch priorities on the fill front, we can pick the patch with the highest priority and select it as the in-paint patch. Let's refer to it as p. The next phase in the inpainting process is to find the patch that is the most similar to the previously chosen patch. The mean squared error was the metric utilized in previous techniques to determine similarity. However, none specify what to do when two (or more) patches have the same mean squared error. In such instances, it was discovered that the algorithm provides visually bad results for some images. Calculating the variance of the patches with the same mean squared error is the solution to this problem. This variance used is the variance of the patch's pixel values in relation to the mean from equation (3.30), of the pixels from the same patch that corresponds to the pixels in the source region of the inpainted patch. (i.e., pixels corresponding to $p \in \phi \cap \Psi$). Equation (3.31) and (3.32) show how to calculate the MSE and the Variance respectively.

$$Mean\ Squared\ Error = \frac{f_{p \in \phi \cap \Psi}}{\#\{p \mid p \in \phi - \Psi\}} \tag{3.31}$$

$$Variance = \frac{\sum (f_{p \in \phi - \Psi} - M)^2}{\#\{p \mid p \in \phi - \Psi\}} \tag{3.32}$$

3.4 Conclusion

In this chapter, the different machine learning techniques employed for experimentation in Computer-Aided Diagnosis of skin cancer are explored. The chapter attempts to break down the mathematical constructs of these methods. An overview of leading hair removal techniques is also presented in this chapter.

Chapter 4
IMPLEMENTATION

4.1 Introduction

Precise segmentation of the lesion region in dermoscopy pictures is critical for improving the efficacy of ensuing stages such as feature extraction and lesion classification, as it significantly impacts their outcomes. Dermatologists can undertake large-scale visual screening exams for the early detection of melanoma illnesses and treatment evaluation using segmented lesions. To correctly diagnose melanoma illness, precise segmentation of the pigmented regions is essential. Segmentation extracts important border structural information from the lesion region, such as asymmetry, diameter, and border irregularity, which is crucial for melanoma diagnosis. Furthermore, key features such as globules, blue-white regions, and an unusual pigment network can only be retrieved when the lesion border is detected accurately. As a result, the lesion segmentation phase is the most important step in detecting melanoma early on. However, detecting lesion borders in dermoscopy pictures is difficult because the noise in the images, such as air bubbles, reflections, skin lines, and hairs, causes significant segmentation mistakes when they are not properly addressed. Aside from the noise, the intensity inhomogeneity and low contrast of the lesion margins degrade the performance of automated skin segmentation algorithms significantly.

The intensity inhomogeneity of dermoscopy images is often related to the acquisition of the image under various lighting conditions. As a result, a robust and reliable automated approach for hair removal from dermoscopic pictures is required for skin region detection in computer-aided diagnosis. This chapter contains a thorough description of the dataset used in the implementation of the experiment, the steps involved in the implementation and the challenges encountered during execution. This chapter also describes the individual steps in this experiment with clear details on each step's composition and relevance. In the experimentation process, images from the ISIC 2018 dataset are first transformed from RGB color space to grayscale. Then for the composite preprocessing step, a Blackhat morphological filter is applied to the bitonal image, thresholding is performed using the Otsu method. The OpenCV telea algorithm is applied for inpainting the hairs in the resultant image. The output of this process in an inpainted image with little to no hair presence. A high-level representation of the various steps for this implementation is shown in figure (4.1). To justify the relevance of the

experiment, the output images (without hair) are parsed as input to a segmentation algorithm. The results of this segmentation process are actively compared to a control experiment conducted with unprocessed images from the ISIC 2018 data set. The two experiments are evaluated with respect to the Jaccard index, and dice coefficient. The Jaccard index can be calculated by dividing the size of the intersection by the size of the sample set's union using equation (4.1).

$$J(A,B) = \frac{|A \cap B|}{|A \cup B|} = \frac{|A \cap B|}{|A| + |B| - |A \cap B|} \tag{4.1}$$

Where,

$$0 \leq J(A,B) \leq 1$$

The dice similarity coefficient (DSC) is defined as a measure of overlap between the true and estimated classes, and it may be determined using equation (4.2).

$$DSC = 2\,\frac{(PPV_i * TP)}{(PPV_i + TP)}\,PPV_i \tag{4.2}$$

Where, PPV_{D} is the Positive Predictive Value (PPV) can be determined using equation (4.3) below, where TP refers to true positives and FP refers to false positives.

$$PPV_i = \frac{TP}{(TP + FP)} \tag{4.3}$$

The results of the experiment are presented and discussed in the subsequent chapter.

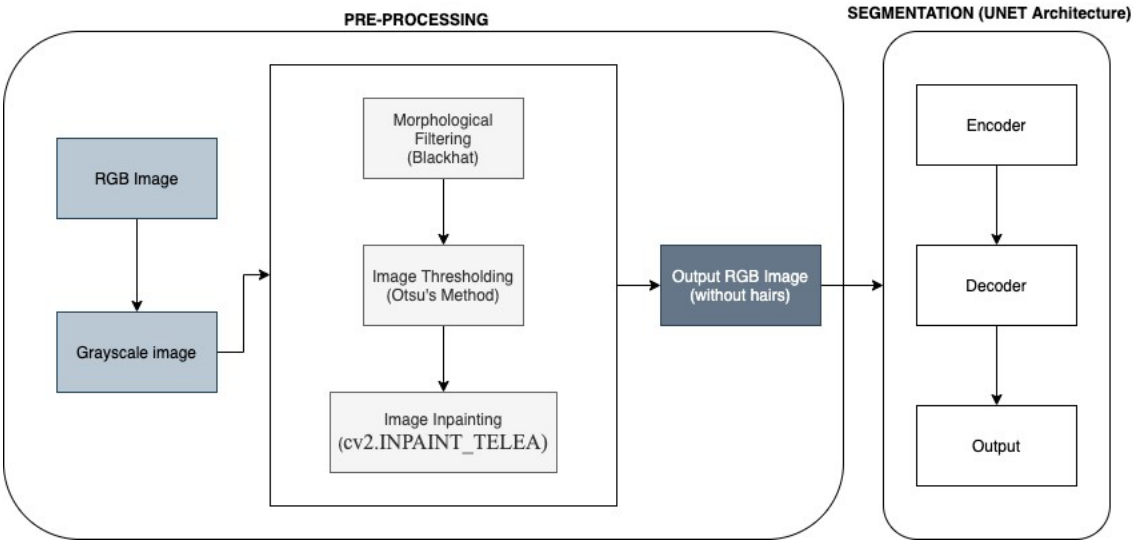

Figure 4.1: High-level representation of the major steps carried out during this experiment

4.2 Dataset Description

This project uses the publicly published dataset by the International Skin Imaging Collaboration (ISIC) for the 2018 competition. The ISIC is a recurring challenge to develop tools for the analysis of images specifically for the automation of segmentation and diagnosis of skin lesions from dermoscopic images. The yearly challenge is broken down into three (3) parts, namely, 1. Lesion Segmentation, 2. Lesion Attribute Detection, and 3. Disease Classification. This dataset consists of 2594 dermoscopic images with ground truth segmentation masks. For validation and test sets, 100 and 1000 images are available respectively without ground truth masks. The images in this dataset have various noise artefact challenges including the presence of hairs, vignettes around image, low contrast images that obstruct lesion boundary identification, among others. These images provide an excellent platform to test the efficiency of our automated image pre-processing model. Figure 4.2 shows the presence of various noise artefacts in images from the ISIC 2018 dataset.

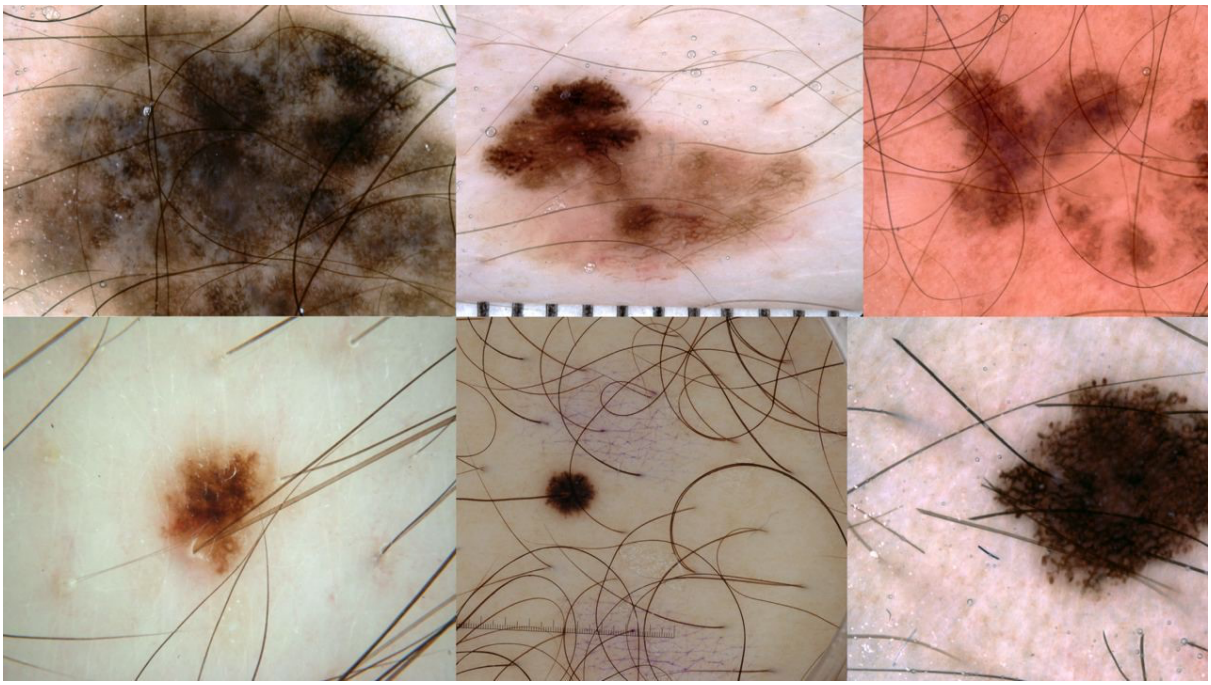

Figure 4.2:Various noise artefacts present in images from the 2018 ISIC dataset

4.3 Overview of Morphological Filtering

Perceptibility and visibility of distinct sections into which an image can be divided are among the goals of image preprocessing. Cleaning the image of various types of noise; improving the contrast between neighboring regions; simplifying the image via selective smoothing or deletion of features at scales; and maintaining only features at certain acceptable scales are some of these goals. While previous techniques to tackling the above goals have primarily relied on linear system tools, there is a growing recognition that linear approaches are not well suited to solving difficulties requiring geometrical features of the image and may even fail. Mathematical morphology is a sophisticated nonlinear methodology that can successfully handle the abovementioned challenges. Mathematical morphology is a set- and lattice-theory-based image analysis method that systematically describes the geometric structure of image objects. It began in the late 1960s intending to analyze geological and biomedical binary image data. Morphological image processing is a set of non-linear processes concerned with the shape or morphology of image features. According to M.S and Nawaz (2017), Morphological procedures rely solely on the relative ordering of pixel values, rather than their numerical values, and are hence well adapted to the processing of binary images. Grayscale images can also be subjected to morphological treatments in which the light transfer functions are unknown and the absolute pixel values are of no or small importance. Morphological approaches use a small form or pattern called a structuring element to explore an image. As shown in figure 4.3,

the structuring element is placed in all locations available in the image and compared to the pixels in its immediate vicinity. Some operations determine if an element "fits" into the neighborhood, while others determine whether it "hits" or intersects it.

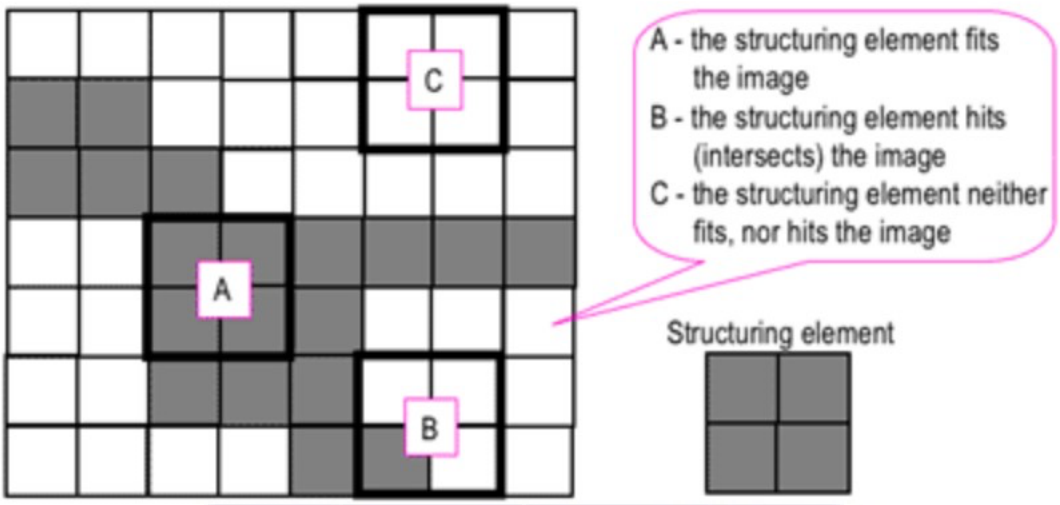

Figure 4.3: Using a structural element to probe an image

4.4 Grayscale Conversion

The color image (RGB color space) is converted to grayscale as shown in figure 4.4, in this phase of our proposed process. The conversion to grayscale images aids in the identification of lesion margins and other dermatological features. Grayscale photos have lower inherent complexity than color photographs since they are essentially different color shades of gray, requiring less information to be provided for each pixel. The most typical approach for converting an RGB color image to a grayscale image is the weighted method, which adds weights based on wavelength to the red, green, and blue channels. The weighted approach, also known as the luminosity method, assigns different weights to red, green, and blue colors based on their wavelengths. The improved formula is given in equation (4.4) as:

$$\text{Grayscale} = 0.299R + 0.587G + 0.114B \tag{4.4}$$

For using the PCT method to convert a three-layer color image into a single-layer grayscale image, only pixels used in the subsequent analysis are considered when determining the weights. As a result, the principal component transform will not include pixels from the black surround. When the near-black pixels in the surround are included, the first principal component will explain a reduced share of the total variance.

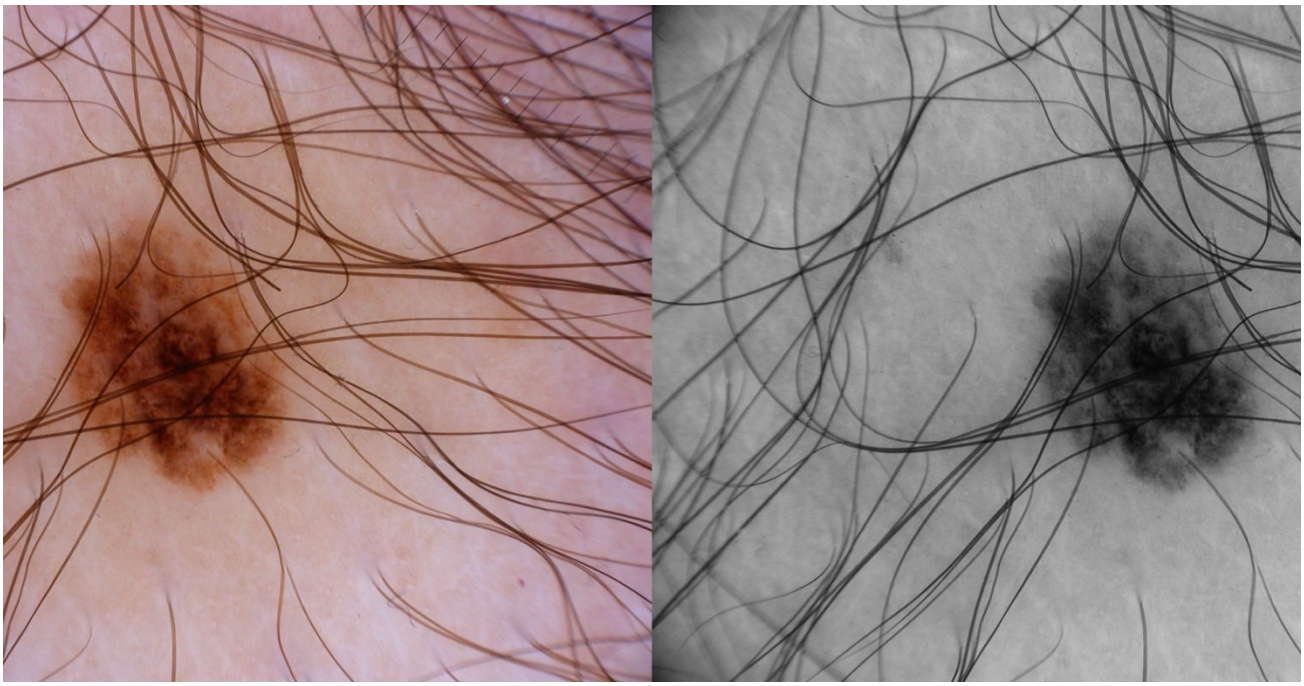

Figure 4.4: Output of grayscale conversion

4.5 Removal of Artefacts – Hairs

All algorithms for segmenting skin lesions must pay special attention to removing artefacts, especially during pre-processing. In this context, artefacts are everything in the image which is not skin or a lesion. Hairs, air bubbles, scales, or felt-pen marks drawn on the skin by the patient or the physician are all examples of artefacts. The existence of hairs is the most significant stumbling block for most algorithms regarding proper segmentation. This is because the color of hair is usually highly similar to the color of the skin lesion. If the hairs are not addressed, they will be categorized as lesions, resulting in inaccurate segmentation and disease classification. The presence of scales and air bubbles, in addition to hairs, might cause erroneous segmentation. Different scale removal techniques are used to remove the scales, but air bubbles usually have no effect on segmentation. The presence of an air bubble alters the color of the skin/lesion below. This color shift, however, is not drastic. Because the air bubbles are usually relatively small, the form of the histogram employed in the segmentation process is unaffected. Hair on the skin surrounding the lesion is a major impediment to accurate lesion segmentation. For the segmentation algorithm, hair is a significant source of confusion. The presence of dark, dense hairs and lighter hairs along the lesion's perimeter will inevitably result in inaccurate segmentation. Although it is feasible to remove hairs with a razor manually, it is vital to keep the method for diagnosing a skin lesion as simple as possible for both the physician and the patient. Filtering is the most straightforward approach to removing hairs in digital

image analysis. Hairs can be filtered out due to their long, thin structure if the filter has the relevant smoothing capabilities or possibly the window size is large enough. In this experiment, morphological techniques are utilized to filter out the hairs.

4.5.1 Blackhat Morphological Filtering

To find hair outlines, a black-hat morphological operation is used concerning direction. Morphological processes such as opening, closure, erosion, and dilation are used to decrease or enhance particular image regions. The black-hat transform creates an image that contains all the objects or elements in an input image that are smaller than the structuring element and darker than their surroundings. The implementation of black-hat morphology in the proposed solution enhances image components with greater structural elements that are darker than their surroundings. A black-hat operation is used to draw attention to darker items (i.e., hair) against a lighter background (i.e., skin tone). It's crucial to choose the proper form and size parameter of the Structuring Element in equation (4.5) to distinguish the hair structures from the grayscale image. The appropriate choice of kernel (size) diameter of the structuring element has been empirically demonstrated to significantly impact hair removal without the influence of hair shadows.

$$SE = strel('diamond', r) \tag{4.5}$$

which creates a diamond-shaped structuring element, where r specifies the distance from the structuring element origin to the points of the diamond, with a 17-pixel diameter distance reduced both thin and thick hair artefacts from gray-scale images, according to studies (M.S. & Nawaz, 2017). The output of the morphological Blackhat filtering can be seen in figure 4.5 below.

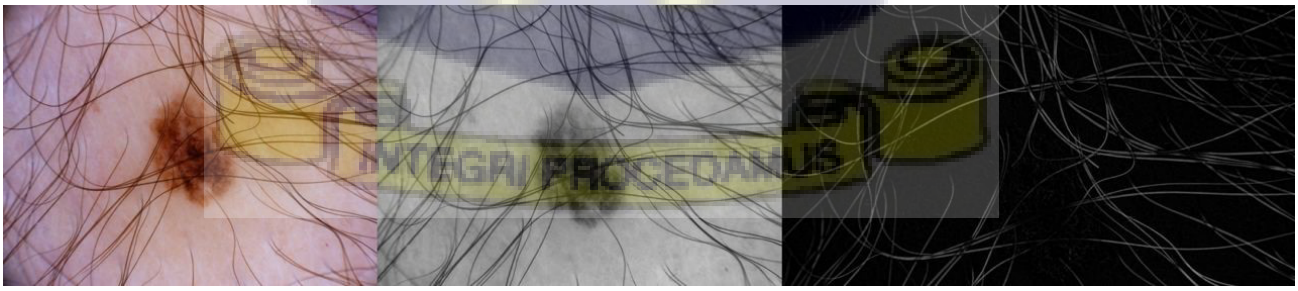

Figure 4.5: Output of Morphological Blackhat filtering

4.5.2 Image Thresholding

Thresholding is an image processing approach that creates a bitonal (also known as binary) image by applying a threshold value to the original image's pixel intensity. It's most typically used on grayscale photographs, although it can also be used on color ones as well. The picture intensity (relative image lightness) threshold is either manually set or automatically set by an application. Pixels with a bit value below the set threshold are transformed to black (bit value of zero), while pixels with a bit value above the set threshold are turned to white (a bit value of one). The thresholding procedure is sometimes regarded as distinguishing foreground (black) and background (white) values in an image as seen in figure 4.6. Simple thresholding actions set one global threshold value for all pixels in an image, regardless of local contrast fluctuations. Further advanced thresholding techniques such as adaptive thresholding sample a smaller and larger number of image regions and set the threshold value appropriately. At a regional level, adaptive thresholding, also known as dynamic or local thresholding, defines the threshold level for deciding whether to convert to white or black. The area sampled and the technique of evaluation differ depending on the application. Compared to global thresholding, adaptive thresholding at the pixel level can produce significantly better results, especially for images with varying regional contrast differences. Thresholding methods may be categorized based on the information they extract from the data. The following are the most popular thresholding methods in the research domain.

- Histogram-shaped techniques
- Object-attribute techniques
- Cluster-based techniques
- Local techniques
- Entropy-based
- Spatial techniques
- Attribute similarity methods

A clustering-based thresholding method is used for this experiment, specifically Otsu's method. Otsu's approach is based on choosing a threshold for dividing an image into two classes with the least variance within each class. The distributions cannot be changed but selecting a threshold number changes the spread between the two halves of the distribution.

The goal is to find a threshold that reduces the total spread. The "within-class" variance can be defined as the weighted sum of the variances of each cluster in equation (4.6).

$$\sigma^2_{within}(T) = n_B(T)\,\sigma^2_B(T) + n_F(T)\,\sigma^2_F(T) \tag{4.6}$$

where:

$$n_B(T) = \sum_{i=0}^{T-1} p(i)$$

$$n_F(T) = \sum_{i=T}^{N-1} p(i)$$

$$\sigma^2_B(T) = The\ variance\ of\ background\ pixels$$

$$\sigma^2_F(T) = The\ variance\ of\ the\ foreground\ pixels$$

The above equations necessitate computing "within-class" variance for every class and every conceivable value for thresholding, which is a very computationally expensive process that should be avoided. The calculation of inter class variance is a less expensive step computationally, and it can be defined as within-class variance deducted from the total variance in equation (4.7).

$$\sigma^2_{Between}(T) = \sigma^2 - \sigma^2_{within}(T) = n_B(T)[\mu_B(T) - \mu]^2 + n_O(T)[\mu_O(T) - \mu]^2 \tag{4.7}$$

Where μ is the combined mean, and σ^2 is the combined variance. The weighted variance of the cluster means around the overall mean is the between-class variance. Substituting in equation (4.8) as:

$$\mu = n_B(T)\mu_B(T) + n_O(T)\mu_O(T) \tag{4.8}$$

To simplify the results, we have the resultant equation (4.9) as:

$$\sigma^2_{Between}(T) = n_B(T)n_O(T)[\mu_B(T) - \mu_O(T)]^2 \tag{4.9}$$

In a nutshell, the algorithm divides the pixels into two groups based on the value for each potential threshold. The mean of each cluster is then calculated, and the difference between the means obtained is squared. Finally, the number of pixels in one cluster is multiplied by the number of pixels. As we iterate over the potential thresholds, it turns out that the threshold computations are not independent., therefore the approach is efficient.

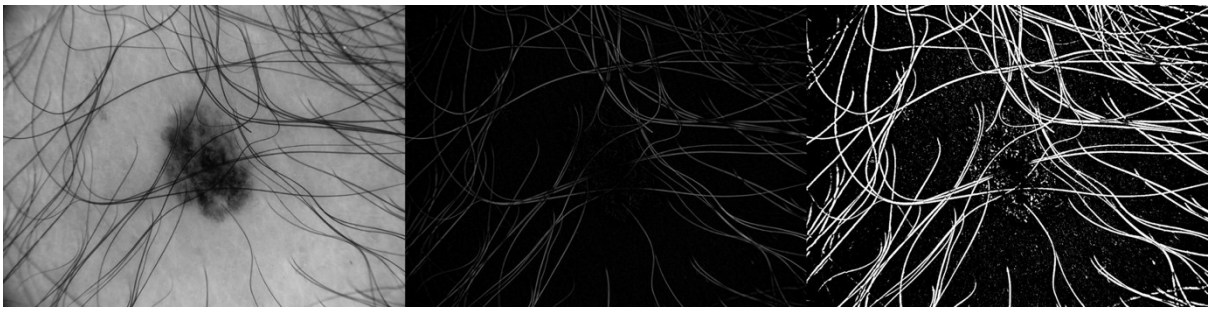

Figure 4.6: Output of thresholding step

4.5.3 Image Inpainting

Inpainting is the art of restoring the fundamentals of visual art to an image. It entails filling in unknown data in a known region of an image with the primary goal of restoring harmony to deprecated images that have been worn down over time or by objects that we want to remove from the image. Hair in dermoscopic images is considered unwanted and should be removed. For this experiment, the OpenCV cv2.INPAINT_TELEA: An image inpainting technique based on the fast-marching method was used. Consider the inpainting of a region in an image; the telea method starts at the region's boundary and gradually moves within it, filling everything in the boundary first. A small neighborhood is required to be inpainted around the pixel on the neighborhood. The normalized weighted sum of all known pixels in the neighborhood is used to replace this pixel. It is critical to select the appropriate weights. Pixels close to the point, near the boundary's normal, and contours are given more weight on the boundary. The algorithm advances to the next closest pixel using the FastMarching Method when a pixel is inpainted. The output image of the previous thresholding step serves as a mask for inpainting with telea. This mask image indicates where the damage in the image exists. The non-zero pixels in the mask image indicate which areas should be inpainted, while the zero pixels are considered as normal (do not require inpainting). Consider figure 9 below, the aim is to inpaint the point p found at the boundary $\partial\Omega$ of the region Ω.

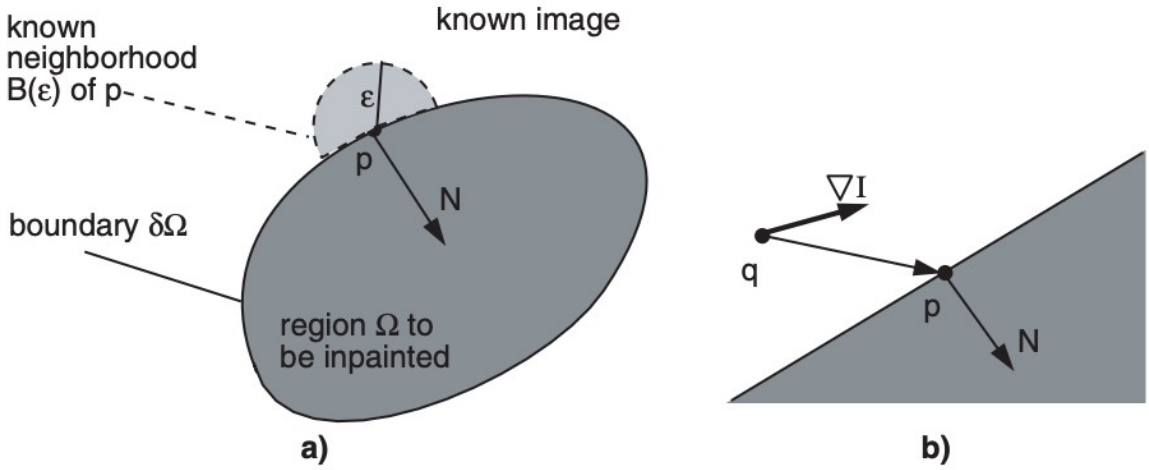

Figure 4.7: The inpainting principle. Image credit:(Telea, 2004)

Given a small neighborhood Bε(p) of size ε of the known image around p (Figure 4.7(a)), the inpainting of p should be determined by the values of the known image points nearest to p. That is, in Bε(p). The algorithm first considers gray value images, then color images. For the minimum value of ε, consider a first-order approximation Iq (p) of the image in point p, given the image I(q) and gradient ∇I(q) values of point q (Figure 4.7(b)):

$$I_q(p) = I(q) + \nabla I(q)(p - q) \tag{4.10}$$

Then, by adding up the estimates of all points q, weighted by a normalized weighting function w(p, q),proceed to inpaint point p as a function of all points q in B(p):

$$I(p) = \frac{\sum_{q \in B_{\epsilon(p)}} w(p,q)[I(q) + \nabla I(q)(p - q)]}{\sum_{q \in B_{\epsilon(p)}} w(p,q)} \tag{4.11}$$

The inpainting of p propagates the gray value and the fine details of the image over B_ε (p), thanks to the weighting function w (p, q).

To in-paint the entire area Ω, we successively apply $I(p)$, eq (4.9) to all of the discrete pixels of $\partial\Omega$ in increasing distance from the beginning location $\partial\Omega i$ then advance the border inside Ω until the entire region is in painted. By inpainting points in order of increasing distance from $i\partial\Omega$ the areas closest to known image points are filled in first, simulating manual inpainting approaches. Figure 4.8 shows examples of applying the FMM based inpainting process with the original images, the thresholding masks and the output of inpainting.

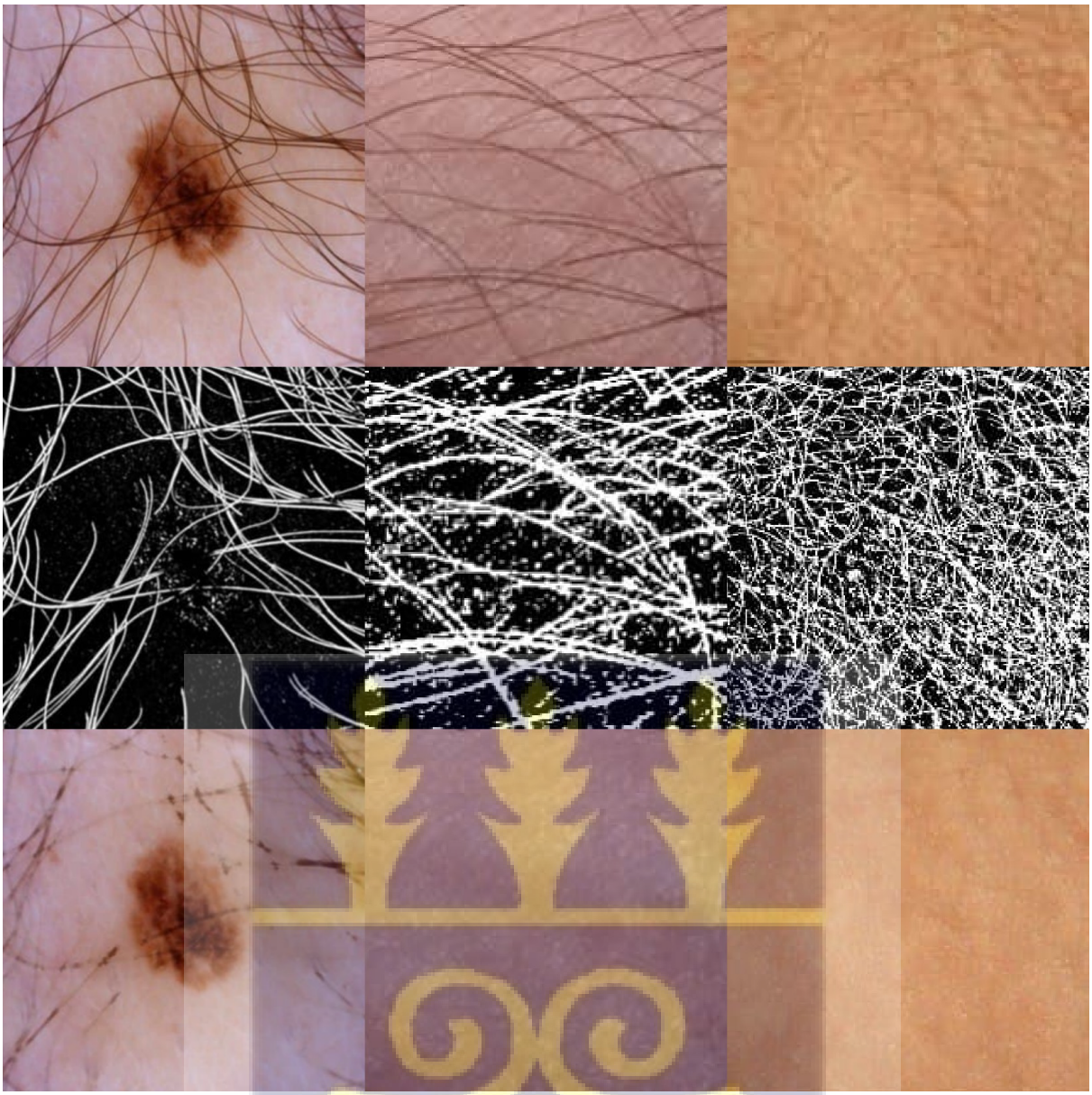

Figure 4.8: Examples of original images, the thresholding masks and the output of inpainting.

4.6 Image Segmentation

One of the most critical and challenging stages in image processing is segmentation. It needs to be quick and precise since the following processes like feature extraction and disease classification are heavily reliant on it. As previously stated, segmenting dermoscopy images is particularly challenging due to various issues, including low contrast between the lesion and healthy skin, color variations within the pigmented region, the presence of hair, and other aberrations. This re-iterates the relevance of the preprocessing steps, especially of hair removal. In this research work, the focus is mainly on hair removal from dermoscopic images obtained from the ISIC 2018 competition. To validate the claim of improving segmentation by increasing

the efficiency of hair removal algorithms, we proceed to segment the image dataset using the U-Net architecture for segmentation as defined in the python library for Bio-Medical Image Segmentation (Olaf Ronneberger et al., 2015). The architecture is divided into two paths. The first path, the contraction path (also known as the encoder), and it is used to capture the image's context. The encoder is essentially a stack of convolutional and maximum pooling layers. The second path is the symmetric expanding path (also known as the decoder), which is used to achieve exact localization using transposed convolutions. As a result, it is an end-to-end fully convolutional network (FCN), which means it only has Convolutional layers and no Dense layers, allowing it to accept images of any size. The convolutional network's contracting path follows the standard convolutional network architecture. It consists of two 3x3 unpadded convolutions that are repeated, each followed by a rectified linear unit (ReLU) and a 2x2 max pooling operation with stride 2 for downsampling. With each level of downsampling, the number of feature channels doubles. A 2x2 convolution ("up-convolution") that halves the number of feature channels, a concatenation with the proportionately cropped feature map from the contracting path, and two 3x3 convolutions, each followed by a ReLU in the expansive path follow an up-sampling of the feature map.

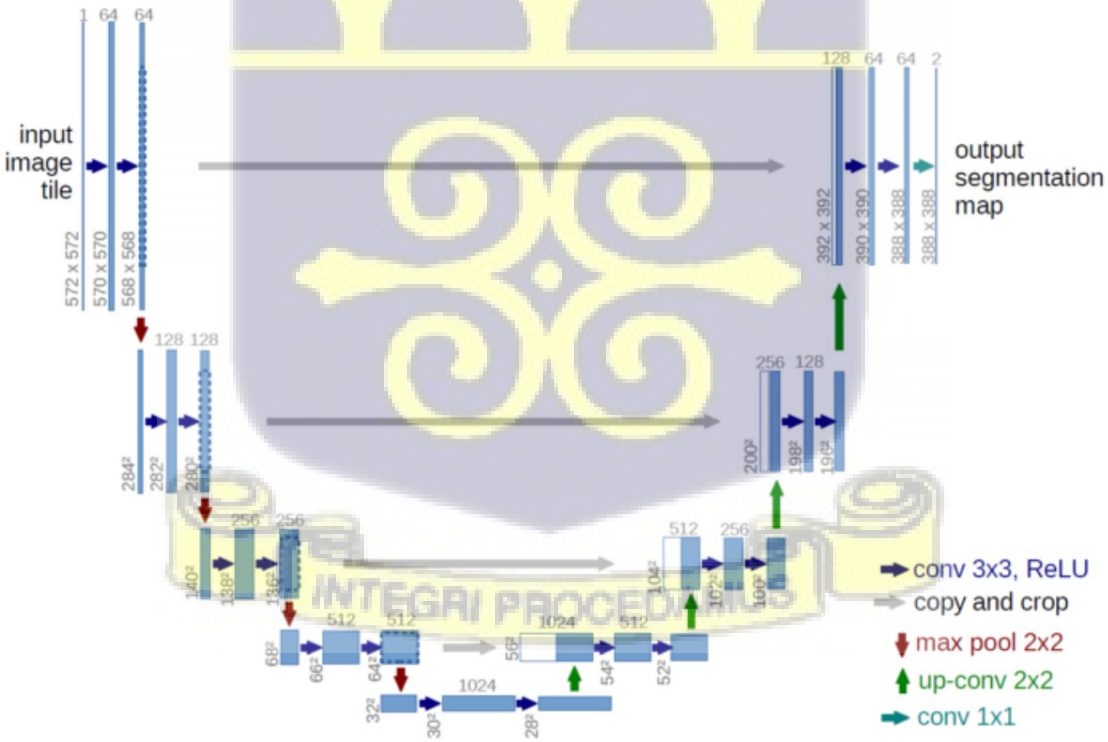

Figure 4.9: U-Net as described in the original research paper by (Olaf Ronneberger et al.,2015)

Each blue box in the Figure 4.9 represents a multi-channel feature map. The number of channels is displayed near the top of the box. On the box's lower left edge, the x-y size is displayed. White boxes denote feature map copies. The arrows represent the different operations. The two alternative methodologies are compared to test the effect of the preprocessing algorithm targeted at hair removal. The same U-Net design is run once with and once without pre-processing. The results of the experiments are presented and discussed in the following chapter.

4.7 Conclusion

This chapter distinctly explains each step in the experimental implementation of hair removal methods toward the improvement of image segmentation results. A full description of the segmentation algorithm implemented is also described in this chapter. The subsequent chapter explains the results of the experiment conducted.

Chapter 5
EVALUATION AND DISCUSSION

5.1 Introduction

The irregular structure of skin lesions complicates skin cancer detection, different shades of colors on each skin, presence of obstructive artefacts such as air bubbles, oil and hairs and pinpointing the region of interest on each dermoscopy image. Expertise in this subject is required to detect minute changes on the skin. On the other hand, the human eye may not always notice these minute variations. Many lives can be saved by assisting doctors with computer vision and deep learning techniques. With this motivation we investigated aiding skin cancer detection by improving on the performance of segmentation with the preamble of increasing the efficiency of pre-processing methods for hair removal. All the experiments' output data revealed that pre-processing images before segmentation and subsequent detection detecting skin cancer malignancy is a tough issue and generalizing a model for all situations necessitates the use of image preprocessing techniques before feeding into any deep learning algorithm. A hair removal algorithm based on an improved morphological filtering technique is presented, implemented, and tested with encouraging results. The algorithm is straightforward, effective, and easy to use. This study focuses on two (2) primary algorithms: the first is focused hair removal and the second is focused on skin lesion segmentation. However, the skin lesion segmentation serves as a test case for the claim made at the inception of this thesis (i.e., improving preprocessing algorithms has a direct effect on improving the results of segmentation algorithms for image processing).

5.2 Hair Removal

In all the scenarios investigated, the hair-removal algorithm works well. A hair-removal algorithm's performance is determined by whether or not it eliminates enough hair for a more efficient segmentation to be carried out and whether or not it also removes hair artefacts in the process. To objectively evaluate the hair removal technique, we could perform a manual detection and removal of all hair pixels and compare the results of segmentation based on the manual and automatic hair removal. It is evident that this would be a laborious and resource-intensive procedure for the evaluation and therefore not practical. Visual examination of the algorithm’s performance is thus used. The result showed no evidence that inaccurate

segmentation was due to poor hair removal technique in 68 training images and 100 test images. Hairs close to the lesion that are not eliminated and so part of the lesion when segmentation is conducted, or sections of the lesion detected as hair replaced by skin-colored pixel values and hence omitted when segmentation is performed, are examples of indicators. When comparing the method offered in this study to the methods presented in Schmid-Saugeon et al. (2003) and Møllersen (2008), as detailed in Chapter 2, the employment of morphological operations emerges as a similar theme across all three works. SchmidSaugeon et al. (2003) and Møllersen (2008) perform morphological operations on binary photographs and compare the original and transformed images using a pre-defined threshold value. The method presented in this study employs morphological operations to grayscale images and proceeds to perform thresholding. Another advantage of grayscaling images before use is that it offers easier detection of objects in an image as opposed to the RGB formatted images (as presented originally in the dataset). The DullRazor method contains three steps: identifying hair pixels, interpolating those pixels with non-hair pixels, and smoothing the final output. Hair-like structures are recognized using gray-levels, and their lengths and widths are evaluated to determine if they are like those of hairs. Bilinear interpolation is used to replace hair-like detected structures with non-hair pixels. The generated image is then flattened to enhance uniformity in the areas where hairs were identified (Kiani & Sharafat, 2011). The DullRazor method was tested on 68 photos in the training sample, but it performed worse than the algorithm presented in this thesis. For DullRazor to eliminate sufficient hair from the images, the threshold value had to be set at the barest minimum and this caused the inclusion of non-hair pixels. It is important to note that the images used in the evaluation of DullRazor were considerably smaller (512 x 486) than those used in this study (1700 x 1700) and therefore a change in the size of the structural elements on DullRazor could result in increased performance.

5.3 Segmentation

The Jaccard Index assesses the segmented images by 5 random folds validation with a 60 percent -40 percent train-test split. Table 5.1 shows the Jaccard index and dice values for five different folds. The neural network is trained using the 200 training photos for each random fold using U-Nets. After training, another 100 test images are given an average Jaccard Index score. This is done using the U-Net architecture without pre-processing (Approach A) as well as with pre-processing (Algorithm B). Approach A produced an average Jaccard Index and dice coefficient scores of 0.53 with standard deviation of 0.02 and 0.70 with standard deviation of

0.02 respectively. Approach B however made average Jaccard Index and dice coefficient scores of 0.62 with 0.05 standard deviation and 0.78 with 0.04 standard deviation respectively. The preprocessing steps (morphological Blackhat filtering, thresholding, and inpainting) clearly enhanced the segmentation results when looking at the output photos. The segmented images that result are noticeably closer to the dataset's ground truth images. To further compare the results of this work, the Jaccard index and dice coefficient values of the Chan-Vese segmentation algorithm which employs kernel-based edge detection for hair removal by Majtner et al. (2016) are included in table 5.1. The evaluation metrics indicate that the output of this experiment is satisfactory to the premise of the project.

For a few selected skin lesion photos, Figure 5.1 compares the skin lesion segmentation techniques. The input RGB image is shown in the first row of the graphic. The Ground Truth is found in the second row (binary mask manually segmented by a dermatologist). Finally, the output of the U-Net trained with algorithms A and B is shown in the third and fourth rows, respectively.

Table 5.1: Comparison of Experimentation Results

	Jaccard Index	**Standard Deviation**	**Dice Coefficient**	**Standard Deviation**
Approach A	0.53	0.2	0.70	0.02
Approach B	0.63	0.05	0.78	0.04
Approach X (Chen-Vese Seg.)	0.63	0.15	0.76	0.12

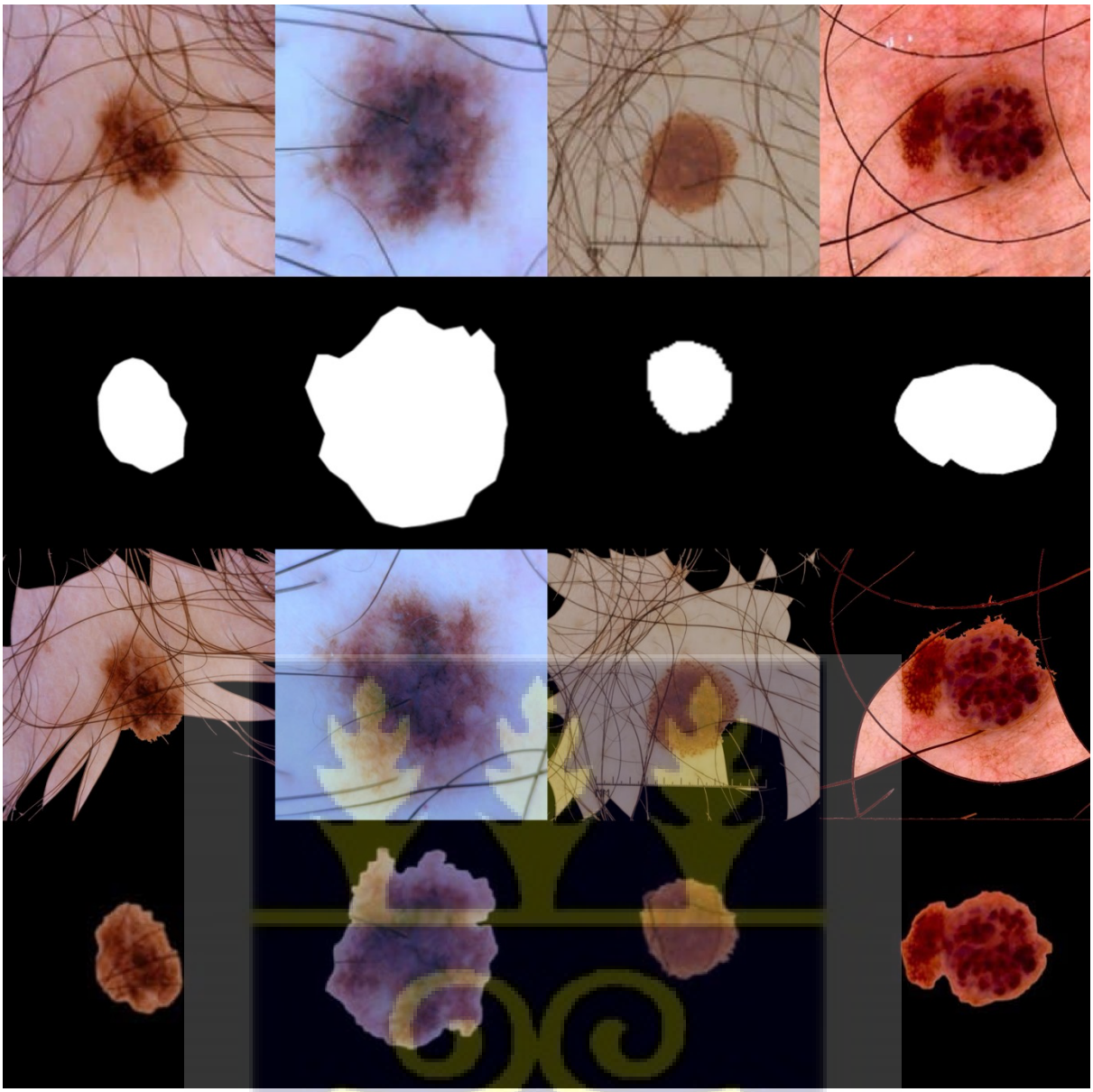

Figure 5.1: Row 1- original images. Row 2- Ground truth from dataset. Row 3- Segmentation output without pre-processing. Row 4- Segmentation output with hair removal

5.4 Challenges

Even though the algorithm produces encouraging results for the high percentage of the photos analyzed, two groups of lesions are incorrectly segmented. When parts of the lesion appear lighter than the skin and are located on the lesion's edges, they fall into one of two groups. The bright area will be considered skin in these circumstances especially when no artefacts are obscuring these areas. Images with several skin lesions in one frame make up the other category. The difficulty may be overcome by allowing the practitioner to specify the lesions count in the image if the lesions are well separated. An over-segmentation occurs when the lesions are close together. In these circumstances, based on the area of the skin mode, the first

and second minimum, it may be able to segment the image pixels into three (3) main classifications. The training and test samples both contain photographs of persons with a lighter complexion. Although this group is most likely to develop melanoma, a darker skin tone is not guaranteed never to develop melanoma. The segmentation algorithm must be evaluated on photos of people with darker skin to ensure that it works better due to the preprocessing techniques used, independent of the patient's skin tone. Suppose it is shown that the algorithm only works on images of individuals with lighter skin tones. In that case, the thesis premise is not universal, and further effort is needed to enhance segmentation algorithms for universal efficiency. This experimentation is considered for future research work.

Chapter 6
CONCLUSION AND FUTURE DIRECTIONS

6.1 Conclusion

Skin cancer has become more common in recent years, especially among white-skinned persons with significant sun exposure. If caught early enough, this cancer can be successfully treated. Early detection and treatment will result in a higher likelihood of survival and lower mortality rates. However, due to subjectivity and the high level of experience physicians require for diagnosis, existing clinical approaches for identifying skin malignancies are prone to human error. As a result, there is a demand for more dependable and precise methods that may benefit both experienced and inexperienced physicians. Because of its usefulness in early detection, dermoscopy is regarded as one of the most important tools in diagnosing skin cancers. With the introduction of computer-aided diagnosis (CAD) in dermoscopy image processing, a new platform for the early detection of skin malignancies was born. In recent years, using computers in melanoma diagnosis has become a prominent study area to assist physicians by providing helpful information about skin lesions. Skin lesion segmentation is vital in developing a computer-aided diagnosis system for skin cancer detection. To achieve efficient segmentation however, studies have shown that is it important to have a robust pre-processing algorithm for removing unwanted artefacts like hair and oil bubble from the images before segmentation. Such artefacts present noise in the images and hinder the efficiency of image processing efforts. The ISIC 2018 dataset is used to evaluate selected hair removal and segmentation algorithms, and the effects of the hair removal method on the output of segmentation are also evaluated. The results of the segmentation of images that the hair removal algorithm had pre-processed are significantly better than that of the output of segmentation without hair removal.

6.2 Future Work

Even after significant pre-processing, the segmentation technique used in this thesis has one fundamental flaw: lesions lighter than the surrounding skin could not be separated successfully. This is a challenge that can be conquered. Light lesions can be discovered by locating the correct bound of the skin mode and then estimating the lesion bound's location. It's also necessary to devise a way to include light areas on the periphery of a darker lesion. Another limitation encountered is the occurrence of multiple lesions within one image frame. This could

also be overcome by adding an optional “multi” input to the segmentation program such that the algorithm knows to detect the furthermost borders of the darker portions of such images. Whether or not this yields a satisfactory result must be tested on a sample of photos with multiple lesions. The hair-removing algorithm works as expected, removing a significant amount of hairs that would otherwise interfere with segmentation, however there is considerable room for further improvement. For hairs outside the lesion, skin-colored pixels are used, while for hairs inside the lesion, lesion-colored pixels are used. If the hair-removing algorithm is to be employed for lesion analysis, a more sophisticated method than morphological filtering is required. Testing the segmentation algorithm on a dataset with images where the skin tone of the patients is darker yet present with lesions needs to be done to justify the effectiveness of the hair removal technique in all scenarios. The performance of the segmentation algorithm may only be evaluated to a certain extent. More lesions from the test sample should be included in the evaluation, and at least one dermatologist should analyze the borders to verify the experiment's output. A bigger training and testing set should be used to improve the output's reliability.

REFERENCES

Abbas, Q., Celebi, M. E., & García, I. F. (2011). Hair removal methods: A comparative study for dermoscopy images. *Biomedical Signal Processing and Control*, *6*(4), 395–404. https://doi.org/10.1016/j.bspc.2011.01.003

Al-masni, M. A., Al-antari, M. A., Choi, M. T., Han, S. M., & Kim, T. S. (2018). Skin lesion segmentation in dermoscopy images via deep full resolution convolutional networks. *Computer Methods and Programs in Biomedicine*, *162*, 221–231. https://doi.org/10.1016/j.cmpb.2018.05.027

Alom, M. Z., Hasan, M., Yakopcic, C., Taha, T. M., & Asari, V. K. (2018). *Recurrent Residual Convolutional Neural Network based on U-Net (R2U-Net) for Medical Image Segmentation*. http://arxiv.org/abs/1802.06955

Alyari, F., & Jafari Navimipour, N. (2018). Recommender systems: A systematic review of the state of the art literature and suggestions for future research. *Kybernetes*, *47*(5), 985–1017. https://doi.org/10.1108/K-06-2017-0196

Attia, M., Hossny, M., Nahavandi, S., & Yazdabadi, A. (2017). Skin melanoma segmentation using recurrent and convolutional neural networks. *Proceedings - International Symposium on Biomedical Imaging*, 292–296. https://doi.org/10.1109/ISBI.2017.7950522

Bi, L., Kim, J., Ahn, E., & Feng, D. (2017). *Automatic Skin Lesion Analysis using Largescale Dermoscopy Images and Deep Residual Networks*. 6–9. http://arxiv.org/abs/1703.04197

Bi, L., Kim, J., Ahn, E., Feng, D., & Fulham, M. (2016). Automated skin lesion segmentation via image-wise supervised learning and multi-scale superpixel based cellular automata. *Proceedings - International Symposium on Biomedical Imaging*, *2016-June*, 1059–1062. https://doi.org/10.1109/ISBI.2016.7493448

Bi, L., Kim, J., Ahn, E., Feng, D., & Fulham, M. (2017). Semi-automatic skin lesion segmentation via fully convolutional networks. *Proceedings - International Symposium on Biomedical Imaging*, 561–564. https://doi.org/10.1109/ISBI.2017.7950583

Brox, T., & Weickert, J. (2004). Level set based image segmentation with multiple regions.

Lecture Notes in Computer Science (Including Subseries Lecture Notes in Artificial Intelligence and Lecture Notes in Bioinformatics), *3175*, 415–423. https://doi.org/10.1007/978-3-540-28649-3_51

Burdick, J., Marques, O., Weinthal, J., & Furht, B. (2018). Rethinking Skin Lesion Segmentation in a Convolutional Classifier. *Journal of Digital Imaging*, *31*(4), 435–440. https://doi.org/10.1007/s10278-017-0026-y

Chakraborty, S., Mali, K., Chatterjee, S., Banerjee, S., Mazumdar, K. G., Debnath, M., Basu, P., Bose, S., & Roy, K. (2017). Detection of skin disease using metaheuristic supported artificial neural networks. *2017 8th Industrial Automation and Electromechanical Engineering Conference, IEMECON 2017*, 224–229. https://doi.org/10.1109/IEMECON.2017.8079594

Chakraverty, S., Sahoo, D. M., & Mahato, N. R. (2019). McCulloch--Pitts Neural Network Model. In *Concepts of Soft Computing: Fuzzy and ANN with Programming* (pp. 167–173). Springer Singapore. https://doi.org/10.1007/978-981-13-7430-2_11

Chan, T. F., & Vese, L. A. (2001). Active contours without edges. *IEEE Transactions on Image Processing*, *10*(2), 266–277. https://doi.org/10.1109/83.902291

Cheng, Y., Liu, W., & Xing, W. (2019). A novel algorithm for exemplar-based image inpainting. *Proceedings of the International Conference on Software Engineering and Knowledge Engineering, SEKE*, *2019-July*, 630–633. https://doi.org/10.18293/SEKE2019-152

Codella, N. C. F., Gutman, D., Celebi, M. E., Helba, B., Marchetti, M. A., Dusza, S. W., Kalloo, A., Liopyris, K., Mishra, N., Kittler, H., & Halpern, A. (2018). Skin lesion analysis toward melanoma detection: A challenge at the 2017 International symposium on biomedical imaging (ISBI), hosted by the international skin imaging collaboration (ISIC). *Proceedings - International Symposium on Biomedical Imaging*, *2018-April*, 168–172. https://doi.org/10.1109/ISBI.2018.8363547

Eltayef, K., Li, Y., & Liu, X. (2017). Detection of Melanoma Skin Cancer in Dermoscopy Images. *Journal of Physics: Conference Series*, *787*, 12034. https://doi.org/10.1088/1742-6596/787/1/012034

Haralick, R. M., Shanmugam, K., & Dinstein, I. H. (1973). Textural features for image classification. *IEEE Transactions on Systems, Man, and Cybernetics*, *6*, 610–621.

Hassan, M., Hossny, M., Nahavandi, S., & Yazdabadi, A. (2017). Skin lesion segmentation using Gray Level Co-occurance Matrix. *2016 IEEE International Conference on Systems, Man, and Cybernetics, SMC 2016 - Conference Proceedings*, 820–825. https://doi.org/10.1109/SMC.2016.7844341

Izadi, S., Mirikharaji, Z., Kawahara, J., & Hamarneh, G. (2018). Generative adversarial networks to segment skin lesions. *Proceedings - International Symposium on Biomedical Imaging*, *2018-April*(Isbi), 881–884. https://doi.org/10.1109/ISBI.2018.8363712

Joseph, S., & Panicker, J. R. (2017). Skin lesion analysis system for melanoma detection with an effective hair segmentation method. *Proceedings - 2016 International Conference on Information Science, ICIS 2016*, 91–96. https://doi.org/10.1109/INFOSCI.2016.7845307

Kawahara, J., Bentaieb, A., & Hamarneh, G. (2016). Deep features to classify skin lesions. *Proceedings - International Symposium on Biomedical Imaging*, *2016-June*, 1397–1400. https://doi.org/10.1109/ISBI.2016.7493528

Lee, T., Ng, V., Gallagher, R., Coldman, A., & McLean, D. (1997). Dullrazor®: A software approach to hair removal from images. *Computers in Biology and Medicine*, *27*(6), 533–543. https://doi.org/10.1016/S0010-4825(97)00020-6

Li, Y., & Shen, L. (2018). Skin lesion analysis towards melanoma detection using deep learning network. *Sensors (Switzerland)*, *18*(2), 1–16. https://doi.org/10.3390/s18020556

Lin, B. S., Michael, K., Kalra, S., & Tizhoosh, H. R. (2018). Skin lesion segmentation: UNets versus clustering. *2017 IEEE Symposium Series on Computational Intelligence, SSCI 2017 - Proceedings*, *2018-Janua*, 1–7. https://doi.org/10.1109/SSCI.2017.8280804

Ma, Z., & Tavares, J. M. R. S. (2016). A Novel Approach to Segment Skin Lesions in Dermoscopic Images Based on a Deformable Model. *IEEE Journal of Biomedical and Health Informatics*, *20*(2), 615–623. https://doi.org/10.1109/JBHI.2015.2390032

Majtner, T., Lidayova, K., Yayilgan, S. Y., & Hardeberg, J. Y. (2016). Improving skin lesion segmentation in dermoscopic images by thin artefacts removal methods. *6th European Workshop on Visual Information Processing, {EUVIP} 2016, Marseille, France, October 25-27, 2016*, 1–6. https://doi.org/10.1109/EUVIP.2016.7764580

Marchetti, M. A., Codella, N. C. F., Dusza, S. W., Gutman, D. A., Helba, B., Kalloo, A., Mishra, N., Carrera, C., Celebi, M. E., DeFazio, J. L., Jaimes, N., Marghoob, A. A., Quigley, E., Scope, A., Yélamos, O., & Halpern, A. C. (2018). Results of the 2016 International Skin Imaging Collaboration International Symposium on Biomedical Imaging challenge: Comparison of the accuracy of computer algorithms to dermatologists for the diagnosis of melanoma from dermoscopic images. *Journal of the American Academy of Dermatology*, *78*(2), 270-277.e1. https://doi.org/10.1016/j.jaad.2017.08.016

Mishra, N. K., & Celebi, M. E. (2016). *An Overview of Melanoma Detection in Dermoscopy Images Using Image Processing and Machine Learning*. 1–15. http://arxiv.org/abs/1601.07843

Møllersen, K. (2008). *Unsupervised Segmentation of Skin Lesions*.

M.S, P., & Nawaz, G. (2017). Reconstruction, Effective Morphological Image Processing Techniques and Image. *International Journal of Trend in Research and Development (IJTRD)*, 1-5.

Mukherjee, S., & Acton, S. T. (2015). Region based segmentation in presence of intensity inhomogeneity using legendre polynomials. *IEEE Signal Processing Letters*, *22*(3), 298–302. https://doi.org/10.1109/LSP.2014.2346538

N, M. P., Sankarie, S. S., & Professor, A. (2020). Survey on Detection of Melanoma Skin Cancer Using Image Processing and Machine Learning. *International Journal of Research and Analytical Reviews*, *7*(1). www.ijrar.org

Nasir, M., Attique Khan, M., Sharif, M., Lali, I. U., Saba, T., & Iqbal, T. (2018). An improved strategy for skin lesion detection and classification using uniform segmentation and feature selection based approach. *Microscopy Research and Technique*, *81*(6), 528–543. https://doi.org/10.1002/jemt.23009

Perez, F., Vasconcelos, C., Avila, S., & Valle, E. (2018). Data augmentation for skin lesion analysis. *Lecture Notes in Computer Science (Including Subseries Lecture Notes in Artificial Intelligence and Lecture Notes in Bioinformatics)*, *11041 LNCS*(i), 303–311. https://doi.org/10.1007/978-3-030-01201-4_33

Pirnog, I., Preda, R. O., Oprea, C., & Paleologu, C. (2015). Automatic lesion segmentation for melanoma diagnostics in macroscopic images. *2015 23rd European Signal Processing Conference, EUSIPCO 2015*, 659–663. https://doi.org/10.1109/EUSIPCO.2015.7362465

Qi, J., Le, M., Li, C., & Zhou, P. (2017). *Global and Local Information Based Deep Network for Skin Lesion Segmentation*. http://arxiv.org/abs/1703.05467

Ridler, T. W., & Calvard, S. (1978). Picture Thresholding Using An Interactive Selection Method. *IEEE Transactions on Systems, Man and Cybernetics*, *smc-8*(8), 630–632.

Romero Lopez, A., Giro-I-Nieto, X., Burdick, J., & Marques, O. (2017). Skin lesion classification from dermoscopic images using deep learning techniques. *Proceedings of the 13th IASTED International Conference on Biomedical Engineering, BioMed 2017*, 49–54. https://doi.org/10.2316/P.2017.852-053

Sabouri, P., & Gholamhosseini, H. (2016). Lesion border detection using deep learning. *2016 IEEE Congress on Evolutionary Computation, CEC 2016*, 1416–1421. https://doi.org/10.1109/CEC.2016.7743955

Sarker, M. M. K., Rashwan, H. A., Akram, F., Banu, S. F., Saleh, A., Singh, V. K., Chowdhury, F. U. H., Abdulwahab, S., Romani, S., Radeva, P., & Puig, D. (2018). SLSDeep: Skin lesion segmentation based on dilated residual and pyramid pooling networks. *Lecture Notes in Computer Science (Including Subseries Lecture Notes in Artificial Intelligence and Lecture Notes in Bioinformatics)*, *11071 LNCS*, 21–29. https://doi.org/10.1007/978-3-030-00934-2_3

Sengupta, S., Mittal, N., & Modi, M. (2019). Improved skin lesion edge detection method using Ant Colony Optimization. *Skin Research and Technology*, *25*(6), 846–856. https://doi.org/10.1111/srt.12744

Senthilkumaran, N., & Rajesh, R. (2009). Edge Detection Techniques for Image Segmentation – A Survey of Soft Computing Approaches. *International Journal of Recent Trends in Engineering*, *1*(2).

Serrano, C., & Acha, B. (2009). Pattern analysis of dermoscopic images based on Markov random fields. *Pattern Recognition*, *42*(6), 1052–1057. https://doi.org/https://doi.org/10.1016/j.patcog.2008.07.011

Simonyan, K., & Zisserman, A. (2015). Very deep convolutional networks for large-scale image recognition. *3rd International Conference on Learning Representations, ICLR 2015 - Conference Track Proceedings*, 1–14.

Sumithra, R., Suhil, M., & Guru, D. S. (2015). Segmentation and classification of skin lesions for disease diagnosis. *Procedia Computer Science*, *45*(C), 76–85. https://doi.org/10.1016/j.procs.2015.03.090

Thoma, M. (2017). *Analysis and Optimization of Convolutional Neural Network Architectures*. *May*. http://arxiv.org/abs/1707.09725

Yang, X., Zeng, Z., Yeo, S. Y., Tan, C., Tey, H. L., & Su, Y. (2017). *A Novel Multi-task Deep Learning Model for Skin Lesion Segmentation and Classification*. 1–4. http://arxiv.org/abs/1703.01025

Yu, L., Chen, H., Dou, Q., Qin, J., & Heng, P. A. (2017). Automated Melanoma Recognition in Dermoscopy Images via Very Deep Residual Networks. *IEEE Transactions on Medical Imaging*, *36*(4), 994–1004. https://doi.org/10.1109/TMI.2016.2642839

Yuan, Y. (2017). *Automatic skin lesion segmentation with fully convolutionaldeconvolutional networks*. 2–5. https://doi.org/10.1109/JBHI.2017.2787487

Yuan, Y., Chao, M., & Lo, Y. C. (2017). Automatic Skin Lesion Segmentation Using Deep Fully Convolutional Networks with Jaccard Distance. *IEEE Transactions on Medical Imaging*, *36*(9), 1876–1886. https://doi.org/10.1109/TMI.2017.2695227

Zhang, Z., Stoecker, W. V, & Moss, R. H. (2000). Border detection on digitized skin tumor images. *IEEE Transactions on Medical Imaging*, *19*(11), 1128–1143. https://doi.org/10.1109/42.896789

Zhao, C., Shuai, R., Ma, L., Liu, W., & Wu, M. (2021). Segmentation of dermoscopy images based on deformable 3D convolution and ResU-NeXt +. *Medical & biological engineering & computing*, *59*(9), 1815–1832. https://doi.org/10.1007/s11517-021-02397-9